

# Chapter 2

## The Nonlinear Dynamics of Calcium

Vivien Kirk and James Sneyd

**Abstract** Oscillations and travelling waves in the concentration of free cytosolic calcium are complex dynamical phenomena that play vital roles in cellular function, controlling such processes as contraction, secretion and differentiation. Although, nowadays, these oscillations and waves may be observed experimentally with relative ease, we still lack a rigorous understanding of, firstly, the mechanisms underlying these waves and oscillations in different cell types, and, secondly, the mathematical structures that underlie these complex dynamics. Thus, the study of calcium waves and oscillations is one area in which modellers have, over the years, played a major role. Here, we review our current understanding of the nonlinear dynamics of calcium waves and oscillations, restricting our attention almost wholly to deterministic models.

### 1 Introduction

In almost every cell type, the concentration of free cytosolic calcium,  $[Ca^{2+}]$ , plays a major role in cellular function and regulation [5, 4]. In all muscle cells, for example, a rise in  $[Ca^{2+}]$  is the signal that causes contraction [8, 40]. In cardiac and skeletal muscle, this rise in  $[Ca^{2+}]$  comes about as  $Ca^{2+}$  enters the cell through voltage-gated channels in the cell membrane. The resultant high  $[Ca^{2+}]$  causes myosin to bind to actin, thus exerting a contractile force. In synapses, where one neuron communicates with another, the release of neurotransmitter is governed by the  $[Ca^{2+}]$  in the presynaptic terminal [96, 99], while in a completely different cell type, the parotid acinar cell (a type of epithelial cell), a rise in  $[Ca^{2+}]$  causes water secretion and thus the production of saliva [1, 155].

In many cell types (hepatocytes, for example) the exact role played by  $Ca^{2+}$  is not well understood, although it seems clear that it is important for cell function,

---

V. Kirk • J. Sneyd (✉)

Department of Mathematics, University of Auckland, Auckland, New Zealand  
e-mail: [v.kirk@auckland.ac.nz](mailto:v.kirk@auckland.ac.nz); [sneyd@math.auckland.ac.nz](mailto:sneyd@math.auckland.ac.nz)

while in other cell types (such as neuroendocrine cells like gonadotropin-releasing hormone neurons) a rise in  $[Ca^{2+}]$  is doubtless closely linked to the secretion of hormone, but we do not understand exactly how this link works [71].

Over the last few decades highly sophisticated methods have been developed to measure  $[Ca^{2+}]$  in cells (often still situated in living animals) both in space and in time. The most important method is undoubtedly fluorescence microscopy. Investigators have developed molecules that emit light when they bind  $Ca^{2+}$ . By loading cells with such  $Ca^{2+}$  fluorescent dyes one is now able directly to observe the  $Ca^{2+}$  in the cell and show the results as a video, for example.

One of the first things that investigators noticed was that, in many cell types, the  $Ca^{2+}$  transients, far from being a simple rise and fall, have complex dynamic behaviour. In some cells,  $[Ca^{2+}]$  oscillates with a period ranging from under a second to many minutes. In other, larger, cells, these oscillations are organised into periodic waves that travel at around  $15 \mu m s^{-1}$ . In even larger cells, such as *Xenopus* oocytes, these periodic waves are organised into periodic spirals or target patterns.

According to current dogma, oscillations and periodic waves of  $Ca^{2+}$  control cellular functions in a frequency-dependent manner.  $Ca^{2+}$  itself is toxic to cells — prolonged high  $[Ca^{2+}]$  will kill a cell — and thus an amplitude-modulated signal is of less use. However, by modulating the frequency of the oscillation, the signal can be carried efficiently, without endangering the cell. Although this is a useful working hypothesis, and is supported by a great deal of experimental evidence, in some cell types the actual situation is considerably more complicated, with both amplitude and frequency playing major roles, while in yet other cell types, the frequency of the oscillation appears to play almost no role at all. Examples of these different situations are discussed in more detail below, and in Fig. 1.

Three examples of  $Ca^{2+}$  oscillations and waves, from three very different cell types, are shown in Fig. 1. In the first example we believe we know what the  $Ca^{2+}$  oscillations are doing, and how their function is controlled by their frequency; in the second example, we believe we know what the  $Ca^{2+}$  oscillations are doing, but it seems that the oscillation frequency is entirely unimportant; in the third example, we think we know what the  $Ca^{2+}$  transients are doing (at least in general terms), but we don't really know how they do it.

In part A of Fig. 1 we show  $Ca^{2+}$  oscillations in airway smooth muscle cells, in response to the agonist methylcholine. These  $Ca^{2+}$  oscillations (indirectly, but through a well-known pathway [73]) cause binding of the contractile proteins, myosin and actin, and thus cause contraction of the muscle [113]. Since airway smooth muscle surrounds the airways, its contraction causes contraction of the airways and restriction of breathing. (Interestingly, there is no other known physiological function of airway smooth muscle; it is the only known organ whose sole function is pathological.) The extent of the muscle contraction is closely correlated with the frequency of the  $Ca^{2+}$  oscillation, and thus we believe we understand the physiological function of these oscillations. Although we call them  $Ca^{2+}$  oscillations, they are, in fact, periodic waves, as can be seen from the more detailed plot in part B. In this space-time diagram, a higher  $[Ca^{2+}]$  is denoted by a

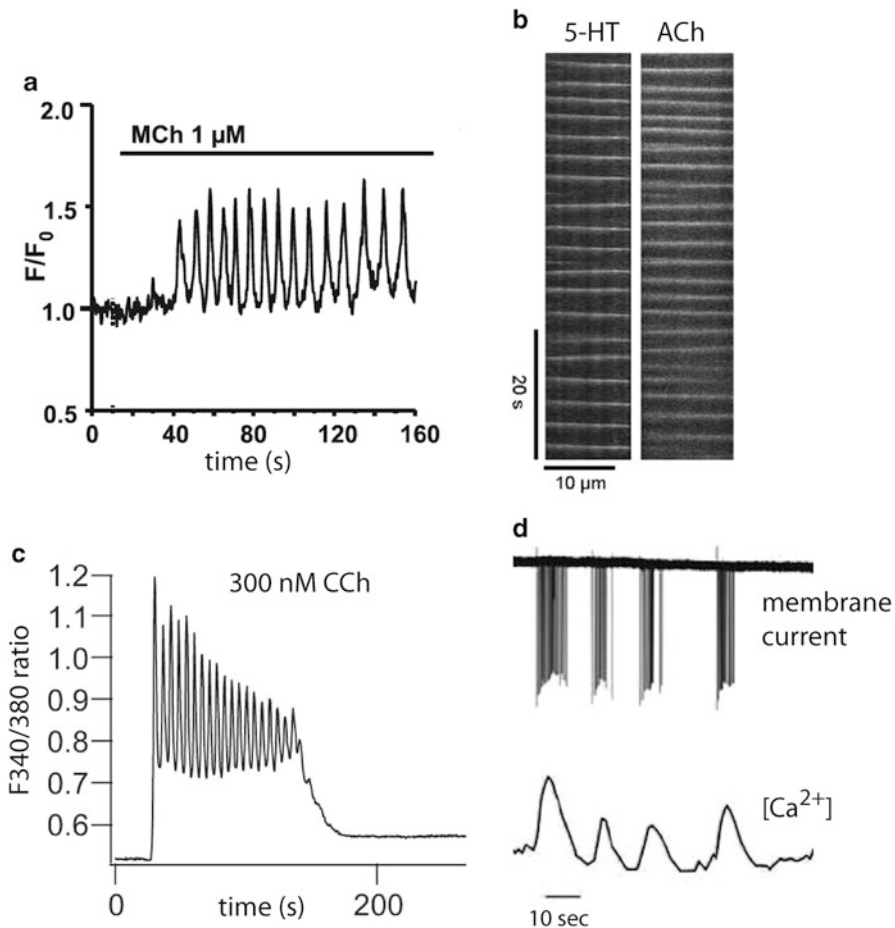


**Fig. 1** Three examples of the complex behaviour of  $[Ca^{2+}]$ . A: Oscillations of  $[Ca^{2+}]$  in human airway smooth muscle cells, in response to the agonist methylcholine (MCh). Figure modified from [107]. B:  $Ca^{2+}$  oscillations in airway smooth muscle cells, plotted in both space and time, showing that the oscillations shown in A are in fact periodic waves. Figure modified from [104]. Responses to two different agonists – serotonin (5-HT) and acetylcholine (ACh) – are shown. C:  $Ca^{2+}$  oscillations in parotid acinar cells, in response to carbachol (CCh). Figure modified from [53]. D:  $Ca^{2+}$  transients in mouse gonadotropin-releasing hormone (GnRH) neurons. Figure modified from [84]. The membrane current (upper trace) and the  $[Ca^{2+}]$  concentration (lower trace) were measured simultaneously. It can be seen that each burst of electrical spikes corresponds to a transient in  $[Ca^{2+}]$

lighter shade; the fact that white bands extend across the domain at a slight angle means that the  $Ca^{2+}$  oscillations are propagating across the cell to form periodic waves.

In part C of Fig. 1 we show  $Ca^{2+}$  oscillations from parotid acinar cells. The parotid gland is one of the saliva-producing glands, and parotid acinar cells are

epithelial cells specialised for the transport of water. Each rise in  $[Ca^{2+}]$  causes the opening of  $Ca^{2+}$ -dependent  $K^+$  channels at one end of the cell, the opening of  $Ca^{2+}$ -dependent  $Cl^-$  channels at the other end of the cell, and thus transcellular ion flow, with water following by osmosis. However, although it was thought for some years that the rate of water flow was controlled by the frequency of the oscillation, this is now thought not to be the case [101, 102]. In this cell type the rate of water transport is governed almost entirely by the average  $[Ca^{2+}]$ , with the frequency of the oscillation playing no important role that we can discern.

Our final example, in part D of Fig. 1, is from a gonadotropin-releasing hormone neuron, a neuroendocrine cell in the hypothalamus that secretes gonadotropin-releasing hormone, or GnRH. The upper trace is the membrane current, which shows clear groups of electrical spikes, usually called electrical bursting. The lower trace shows the associated  $Ca^{2+}$  transient. Periodicity is not clear, so we do not call these  $Ca^{2+}$  oscillations. Although we know that these  $Ca^{2+}$  transients are associated with the secretion of GnRH, we do not understand exactly how. The secretion of GnRH appears to be controlled on a time scale of hours, while these  $Ca^{2+}$  transients occur with much shorter period, on the order of tens of seconds. How the fast  $Ca^{2+}$  transients are connected to the slow control of GnRH secretion is one of the great puzzles in the study of neuroendocrine cells.

It is clear from even this highly selective set of examples that the study of  $Ca^{2+}$  oscillations has a great deal to offer the mathematical modeller. Such complex dynamic phenomena simply cannot be properly understood without detailed quantitative models, and without a detailed understanding of the mechanisms that can drive periodic behaviour. Because of this, mathematical modellers have often played significant roles in the study of  $Ca^{2+}$  dynamics [38, 39, 44, 114, 136].

## 1.1 *Some background physiology*

Although it is not the purpose of this article to present a detailed discussion of  $Ca^{2+}$  physiology, some details are necessary in order to understand how models are constructed.

Because high  $[Ca^{2+}]$  is toxic, all cells spend a great deal of energy ensuring that  $[Ca^{2+}]$  is kept low. This is not an easy job, energetically speaking. All cells are bathed in a  $Ca^{2+}$ -rich environment, with a concentration of approximately 1 mM, kept at this level by continual release from the bones. However, inside the cell cytoplasm, energy-consuming pumps are continually removing  $Ca^{2+}$  to keep  $[Ca^{2+}] \approx 50$  nM, about 20,000 times lower than outside the cell. There is thus an enormous concentration gradient from the outside to the inside of the cell. Hence, cells can raise  $[Ca^{2+}]$  quickly, merely by opening  $Ca^{2+}$  channels in the cell membrane, but must continually expend energy to maintain this concentration gradient.

Internal cellular compartments, such as the endoplasmic (or, in muscle cells, the sarcoplasmic) reticulum (ER or SR) are also major  $\text{Ca}^{2+}$  stores, with  $\text{Ca}^{2+}$  pumps, called SERCA pumps (Sarcoplasmic/Endoplasmic Reticulum Calcium ATPases) continually pumping  $\text{Ca}^{2+}$  from the cytoplasm into the ER or SR. Similarly, the mitochondria constitute another major internal  $\text{Ca}^{2+}$  store.

Thus a cell at rest is continually expending large amounts of energy, merely to keep  $[\text{Ca}^{2+}]$  low, and there is a continual low-level cycling of  $\text{Ca}^{2+}$  into and out of the cytoplasm, as  $\text{Ca}^{2+}$  leaks in, and is then removed by the pumps.

As an additional control for  $[\text{Ca}^{2+}]$ , of every 1000  $\text{Ca}^{2+}$  ions entering the cytoplasm, approximately 999 are quickly bound to large proteins, called  $\text{Ca}^{2+}$  buffers, thus preventing the  $\text{Ca}^{2+}$  from harming the cell. This so-called  $\text{Ca}^{2+}$  buffering can play a major role in quantitative models (although it can have less effect on the qualitative dynamics) and often needs to be considered carefully.

To construct a model of  $\text{Ca}^{2+}$  dynamics one writes down a conservation equation that keeps track of all the  $\text{Ca}^{2+}$  entering and leaving the cytoplasm. There are a number of such  $\text{Ca}^{2+}$  fluxes (some of which, but not all, are summarised in Fig. 2).

- $\text{Ca}^{2+}$  can flow into the cell from outside through a number of types of channel.
  - Voltage-gated  $\text{Ca}^{2+}$  channels open in response to an increase in the potential difference across the cell membrane. The resultant influx of  $\text{Ca}^{2+}$  will lead to further depolarisation and possibly to an action potential if the cell is electrically excitable.
  - Receptor-operated channels open in response (possibly quite indirectly) to the binding of agonist to a cell membrane receptor.
  - Store-operated channels open in response to a severe depletion of the ER or SR.
- $\text{Ca}^{2+}$  is moved from the cytoplasm to outside the cell by the action of  $\text{Ca}^{2+}$  ATPase pumps in the cell membrane. Other ways in which  $\text{Ca}^{2+}$  is removed from the cytoplasm — for example, by a Na/Ca exchanger — are important in some cell types.
- Release of  $\text{Ca}^{2+}$  from the ER or SR occurs through two major channels.
  - When an agonist binds to a receptor on the cell membrane it initiates a series of reactions that ends in the production of inositol trisphosphate ( $\text{IP}_3$ ), which diffuses through the cytoplasm and binds to  $\text{IP}_3$  receptors (IPR) located on the membrane of the ER or SR. IPR are also  $\text{Ca}^{2+}$  channels, and when  $\text{IP}_3$  binds they open, and release  $\text{Ca}^{2+}$  from the ER. Both  $\text{Ca}^{2+}$  and  $\text{IP}_3$  modulate the open probability of the IPR. IPR exhibit the important property of  $\text{Ca}^{2+}$ -induced  $\text{Ca}^{2+}$  release, or CICR, whereupon a small increase in  $[\text{Ca}^{2+}]$  leads to the opening of the IPR and the further release of  $\text{Ca}^{2+}$ . Thus, CICR is a positive feedback process in which  $\text{Ca}^{2+}$  stimulates its own release. In addition, a high  $[\text{Ca}^{2+}]$  will close the IPR.
  - Ryanodine receptors (RyR) are similar to IPR, and are almost as ubiquitous. They are not opened by  $\text{IP}_3$ , but their open probability is modulated by  $\text{Ca}^{2+}$  in a manner similar to IPR. RyR also exhibit CICR, and indeed were the original

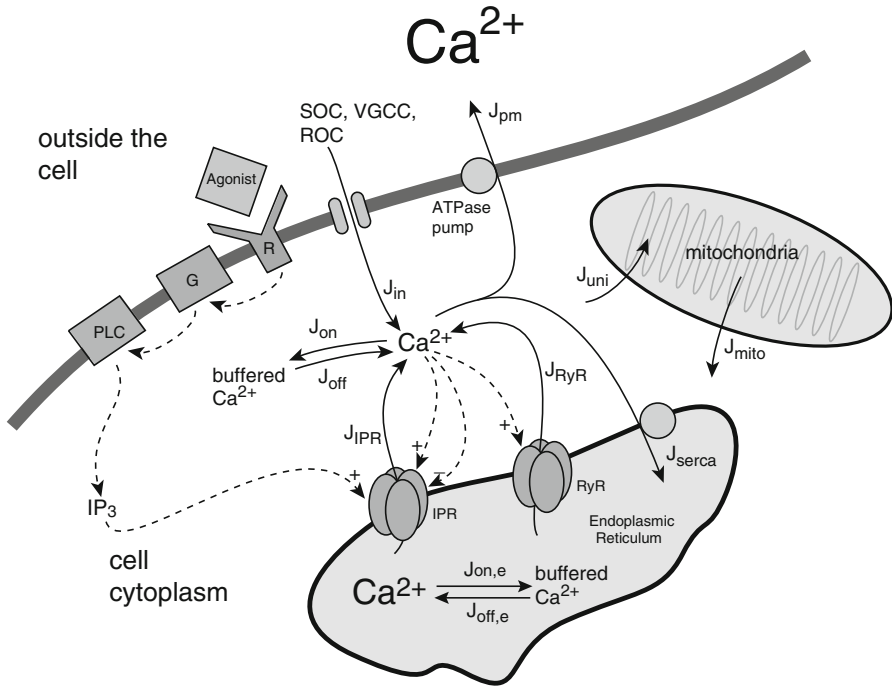


**Fig. 2** Diagram of the major fluxes involved in the control of  $[Ca^{2+}]$ . Binding of agonist to a cell membrane receptor (R) leads to the activation of a G-protein (G), and subsequent activation of phospholipase C (PLC). This cleaves phosphatidylinositol bisphosphate into diacylglycerol and inositol trisphosphate ( $IP_3$ ), which is free to diffuse through the cell cytoplasm. When  $IP_3$  binds to an  $IP_3$  receptor (IPR) on the endoplasmic reticulum (ER) membrane it causes the release of  $Ca^{2+}$  from the ER, and this  $Ca^{2+}$  in turn modulates the open probability of the IPR and ryanodine receptors (RyR). Calcium fluxes are denoted by solid arrows. Calcium can be released from the ER through IPR ( $J_{IPR}$ ) or RyR ( $J_{RyR}$ ), can be pumped from the cytoplasm into the ER ( $J_{serca}$ ) or to the outside ( $J_{pm}$ ), can be taken up into ( $J_{uni}$ ), or released from ( $J_{mito}$ ), the mitochondria, and can be bound to ( $J_{on}$ ), or released from ( $J_{off}$ ),  $Ca^{2+}$  buffers. Entry from the outside ( $J_{in}$ ) is controlled by a variety of possible channels, including store-operated channels (SOC), voltage-gated calcium channels (VGCC), and receptor-operated channels (ROC)

type of  $Ca^{2+}$  channel in which this behaviour was discovered [41]. RyR are the predominant  $Ca^{2+}$  release channels in skeletal and cardiac muscle.

- Reuptake of  $Ca^{2+}$  into the ER/SR is done by SERCA pumps, which use the energy of ATP to pump  $Ca^{2+}$  up its concentration gradient.
- There are also important  $Ca^{2+}$  fluxes to and from the mitochondria. However, we shall not be considering such fluxes in detail here, as they tend to play less important roles in many current models of  $Ca^{2+}$  dynamics. As always, there are multiple exceptions to this rule [23, 24, 31, 45, 59, 91, 92, 95, 106].

Given these fluxes, one possible mechanism of  $\text{Ca}^{2+}$  oscillations becomes a little clearer. When an agonist binds to its receptor it begins the process that results in the production of  $\text{IP}_3$ . This initiates an explosive release of  $\text{Ca}^{2+}$  from the ER/SR, via a process of CICR. Once  $[\text{Ca}^{2+}]$  is high enough the IPR shuts and  $\text{Ca}^{2+}$  efflux from the ER/SR is terminated. As long as the IPR enters a refractory state, thus preventing immediate reopening,  $\text{Ca}^{2+}$  pumps can remove  $\text{Ca}^{2+}$  from the cytoplasm and the cycle can repeat. A similar process occurs through the RyR also, and in many cases both IPR and RyR collaborate to produce the oscillations [133, 146, 149].

It is important to note that there are some cell types, most notably skeletal and cardiac muscle, in which CICR is crucial for cellular function, but does not result in sustained  $\text{Ca}^{2+}$  oscillations. In skeletal and cardiac muscle, the entry of a small amount of  $\text{Ca}^{2+}$  through voltage-gated channels (in response to electrical depolarisation) initiates CICR through RyR, which releases a large amount of  $\text{Ca}^{2+}$  into the cytoplasm, activating the contractile machinery and leading to contraction of the cell. However, each  $\text{Ca}^{2+}$  transient is caused by an action potential which is generated elsewhere – for cardiac cells this is the sino-atrial node – and thus the muscle cell itself exhibits no intrinsic oscillatory behaviour, at least under normal conditions. It is possible to force cardiac cells into a regime where the ER is overloaded with  $\text{Ca}^{2+}$ , and will thus generate spontaneous rhythmic  $\text{Ca}^{2+}$  transients, but this is pathological behaviour. For this reason we shall spend less time here considering  $\text{Ca}^{2+}$  dynamics in cardiac and skeletal muscle. Interested readers are referred to the comprehensive reviews of [8, 40].

We have described above one possible mechanism that can cause  $\text{Ca}^{2+}$  oscillations. However, there are many others [30, 44, 73, 114]. For example,  $\text{Ca}^{2+}$  can affect the production and the degradation of  $\text{IP}_3$ , forming both positive and negative feedback loops which are theoretically capable [37, 105] of generating oscillations (Fig. 3).

It is very important to understand that, although  $\text{Ca}^{2+}$  oscillations may look quite similar in different cell types, with similar periods and shapes, such similarity in appearance can be quite deceptive. Different cell types can, and in general do, have quite different mechanisms generating their  $\text{Ca}^{2+}$  oscillations, and it is unwise to extrapolate mechanisms from one cell type to another, based solely on a desire for simplicity and a fortuitous convergence of appearance. Thus, although the basic toolbox (see section 2) is the same from one cell to another, the way in which those tools are combined and used can be quite different, and each cell must be treated on its own merits.

When  $\text{Ca}^{2+}$  release occurs in a particular part of the cytoplasm,  $\text{Ca}^{2+}$  can diffuse to neighbouring release sites (either IPR or RyR) and initiate further release of  $\text{Ca}^{2+}$  there, thus propagating a travelling wave of increased  $[\text{Ca}^{2+}]$ . In such a way are oscillations converted to periodic waves. These waves travel at approximately  $10\text{--}15\ \mu\text{ms}^{-1}$  and, in larger cell types such as the *Xenopus* oocyte, can form spiral waves and target patterns [83]. Calcium waves can also travel between cells, in regions extending over many cells [85], although this review shall not discuss such intercellular waves at all.

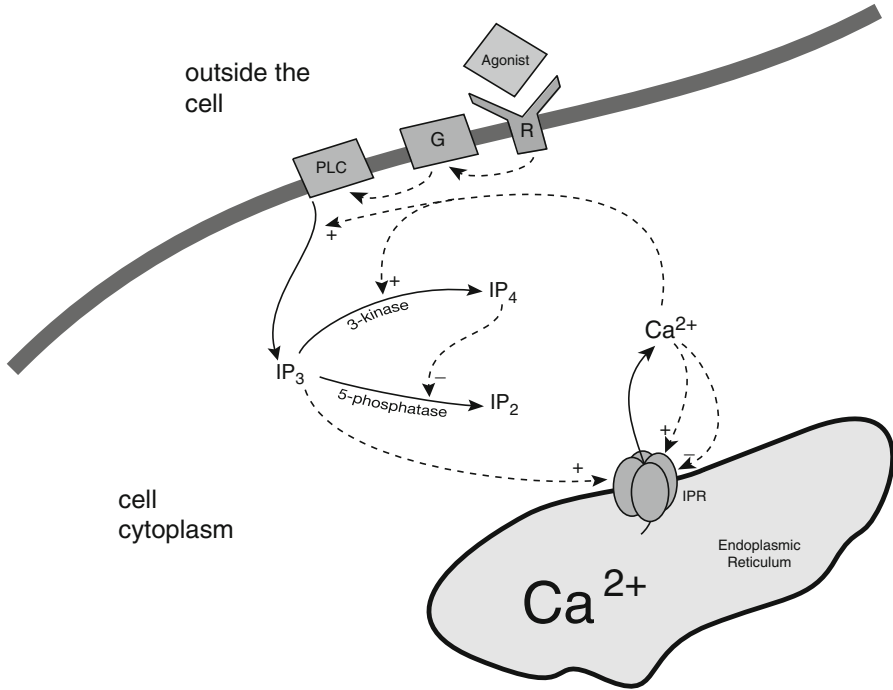


**Fig. 3** Schematic diagram of some of the interactions between  $\text{Ca}^{2+}$  and  $\text{IP}_3$ . Calcium can activate PLC, leading to an increase in the rate of production of  $\text{IP}_3$ , and it can also increase the rate at which  $\text{IP}_3$  is phosphorylated by the 3-kinase. The end product of phosphorylation by the 3-kinase,  $\text{IP}_4$ , acts as a competitive inhibitor of dephosphorylation of  $\text{IP}_3$  by the 5-phosphatase. Not all of these feedbacks are significant in every cell type

It is not the purpose of this review to enumerate and discuss all the possible ways in which  $\text{Ca}^{2+}$  oscillations and waves are thought to arise in different cell types, as this would be a Herculean task. Instead we shall focus on a mathematical analysis of a few of the major mechanisms. The techniques we discuss here will be equally applicable to all the other oscillatory mechanisms and models.

The variety of mechanisms underlying  $\text{Ca}^{2+}$  oscillations and waves is matched by their variety of physiological function. We have already seen specific examples of how  $\text{Ca}^{2+}$  oscillations control the contraction of smooth muscle, the transport of water by exocrine epithelia and the secretion of hormones. However,  $\text{Ca}^{2+}$  oscillations are also known to control fertilisation, proliferation, cell metabolism, vesicle secretion, and even information processing in neurons. Again, we shall not discuss such matters in this review, but refer instead to the many excellent reviews on the topic [4, 5, 39, 44].



## 1.2 Overview of calcium models

There are two major types of model of  $\text{Ca}^{2+}$  dynamics: the spatially homogeneous model, which assumes a well-mixed cell and uses ordinary differential equations, and the spatially inhomogeneous model, which allows for spatial variation of  $[\text{Ca}^{2+}]$  and uses partial differential equations (usually a reaction-diffusion equation). Within each of these divisions, models can be deterministic or stochastic, and can be essentially arbitrarily complex. PDE models, in particular, can become extremely complex, with microdomains of  $\text{Ca}^{2+}$ , i.e., small localised regions where, because of geometric restrictions, the  $\text{Ca}^{2+}$  concentration is orders of magnitude higher than in other parts of the cell.

It is important to note that the type of model one constructs is not essentially dependent on what is believed to be the “real” situation. For example, it is perfectly well known that cells are not well mixed, and that  $[\text{Ca}^{2+}]$  is not even close to homogeneous. Nevertheless, a well-mixed model can still be a useful tool, guiding new experimental results and making testable predictions. Similarly, we know also that, at the highest level of detail, the release of  $\text{Ca}^{2+}$  through either IPR or RyR is inherently a stochastic, not a deterministic process. In some situations this matters, and stochastic models must be used. In other cases, stochastic aspects are less important.

In other words, we construct models, not to be the most detailed and accurate representation of what we believe is the true situation, but to be useful tools to guide our understanding. Depending on what we wish to understand, we construct a model to suit our needs. This is something that is worth emphasising. It is not uncommon for models to be criticised for omitting aspects that exist in the real cell. Since it is hardly possible for models to do otherwise, such criticisms are facile. What really matters is whether or not the model contains the mechanisms that matter for the particular question under investigation.

Conversely, modellers commonly make an analogous mistake; often they construct a model, show that some solutions look the same as experiments, and claim success. This is, of course, equally as facile as the criticisms mentioned above. A similarity of appearance is rarely a guide to underlying mechanism. It is not until the model is used as a predictive tool, and not until experiments are done to test these model predictions, that a model is useful. It matters not whether the experiments confirm or reject the model predictions. The important thing is that the model has been used to advance our understanding.

Whether the model consists of ODEs or PDEs, the basic approach is similar. There are certain cellular components which tend to be common across all cell types, and have reasonably standard models. For instance, the SERCA pumps that transport  $\text{Ca}^{2+}$  from the cytoplasm, up its concentration gradient into the ER or SR, are ubiquitous, and tend always to be modelled in similar ways. Similarly, there are voltage-gated  $\text{Ca}^{2+}$  channels, IPR and RyR,  $\text{Ca}^{2+}$  buffers, and various other  $\text{Ca}^{2+}$  channels, pumps and exchangers, each of which tends to come with a relatively well-accepted model.

Thus, one useful concept is that of a  $\text{Ca}^{2+}$  “toolbox” [6]. This toolbox contains a variety of  $\text{Ca}^{2+}$  transport mechanisms, or modules, from which we can select the most appropriate to build a model in any particular situation. The question of model construction then comes down, in essence, to selection of which modules are the best to use (given the question under consideration), and which is the best model to use for each module. Of course, since there are a very large number of modules in our  $\text{Ca}^{2+}$  toolbox, and many models for each module, one can obtain almost infinite variety.

### 1.3 Stochastic versus deterministic models

One of the major current questions in the field of  $\text{Ca}^{2+}$  modelling is whether to use a stochastic or a deterministic model, and this is a question where the “reality” of the cell’s behaviour is of less use than one might think.

High resolution measurements of  $\text{Ca}^{2+}$  concentration have shown that, in many cell types (most likely all relevant cell types), at low agonist concentrations  $\text{Ca}^{2+}$  release occurs as a series of small, punctate releases, either from a single IPR (a  $\text{Ca}^{2+}$  blip), a group of IPR (a puff) or a group of RyR (a spark) [12, 15, 17, 22, 60, 94, 135, 154]. These releases occur stochastically, due to the stochastic opening and closing of the IPR or RyR. If release from one cluster of IPR is large enough,  $\text{Ca}^{2+}$  can spread to neighbouring clusters of IPR, initiating puffs there, and all the puffs can combine into a global wave [120, 152].

One can now imagine a stochastic scenario for the generation of periodic  $\text{Ca}^{2+}$  waves. Every so often, just by random chance, one cluster will fire strongly enough to initiate such a global wave. Once the  $\text{Ca}^{2+}$  concentration returns to baseline after the wave, there will be a random waiting time before the next cluster initiates the next wave, and thus the waiting time between waves, i.e., the wave period, is set by the waiting time between cluster firings, not by any deterministic limit cycle in the dynamics of the cluster.

Such a stochastic mechanism is relatively easily identified experimentally. A purely stochastic wave activation process will result in the wave initiation times being distributed in a Poisson distribution, in which the mean is equal to the standard deviation. Thus, if a plot of the mean wave period versus the standard deviation (for a variety of waves of different periods, found, for example, by using different agonist concentrations) sits close to the line  $y = x + b$ , for some  $b > 0$ , this is a clear indication that the waves are being initiated by a Poisson process, with a refractory period (presumably set by some other deterministic process) of  $b$ . Note, of course, that if the waves are generated by a purely deterministic process, the standard deviation of the period (for each fixed agonist concentration) is zero.

When one measures the ratio of the mean to the standard deviation (i.e., the *coefficient of variation*, or CV) of the distribution of wave periods, in many cell types the CV turns out to be close to 1. Even for oscillations like those shown in

Fig. 1A, which look to the naked eye as if they are generated by a deterministic process, more detailed studies show that, for a range of  $\text{IP}_3$  concentrations, the CV is close to 1 (unpublished results), and thus these oscillations are initiated by a Poisson process. Similar results are found in other cell types [120, 137]. Hence, the weight of evidence suggests that most, and probably all,  $\text{Ca}^{2+}$  waves are generated by a stochastic, rather than a deterministic process.

However, although this might be the case in reality, the implications for modelling are not clear. It might be tempting to discard all deterministic models as being “wrong”, but this would be a poor solution to a difficult question. As is already well established, all models are “wrong”, but many remain useful. In fact, deterministic models, despite their lack of stochastic reality, do seem to abstract and describe mechanisms that are crucial for oscillations. Deterministic models have been used in a variety of cell types to make predictions about cell behaviour, and these predictions have been confirmed experimentally, leading, for example, to greatly increased understanding of the interplay between RyR and IPR in airway smooth muscle [149], or the role of  $\text{Ca}^{2+}$  influx [129].

Recently, a consensus has begun emerging in the  $\text{Ca}^{2+}$  modelling community that both stochastic and deterministic models are valuable, and that both are needed for a complete understanding of how  $\text{Ca}^{2+}$  oscillations are generated and controlled. Both are, in essence, putting a face on the actual underlying mechanisms — pumping of  $\text{Ca}^{2+}$  into the ER, depletion of the ER,  $\text{Ca}^{2+}$  fluxes through IPR and RyR, and so on — and although the faces differ in detail, the machinery behind them remains similar in many respects. Thus a deterministic model, although ignoring the details of stochastic wave initiation, can remain a highly useful predictive tool, while stochastic models can, in their turn, provide a more solid understanding of exactly how and when each  $\text{Ca}^{2+}$  spike occurs.

So, with the caveat that deterministic models of  $\text{Ca}^{2+}$  oscillations and waves must be approached with care, and one should never have too much faith in their immediate physical reality, in the remainder of this article we shall restrict our attention to just such models.

## 1.4 Excitability

One of the most important features of  $\text{Ca}^{2+}$  dynamics is the property of  $\text{Ca}^{2+}$  excitability [74, 88], where a small amount of  $\text{Ca}^{2+}$  release initiates the release of a larger amount of  $\text{Ca}^{2+}$ , in a positive feedback process. When first discovered in skeletal muscle this property was called  $\text{Ca}^{2+}$ -induced  $\text{Ca}^{2+}$  release, or CICR [41].

CICR can arise in two different ways. Firstly, it can arise through modulation by  $\text{Ca}^{2+}$  of the IPR or RyR open probability; for example, the open probability curve of the IPR is bell-shaped, increasing at low  $\text{Ca}^{2+}$  concentrations, and decreasing at high  $\text{Ca}^{2+}$  concentrations. Thus, at low  $\text{Ca}^{2+}$  concentrations, an increase in  $\text{Ca}^{2+}$  concentration leads to an increase in the open probability of the IPR, and hence positive feedback. The details differ between IPR subtypes, but the qualitative

behaviour is similar ([50] shows a wide selection of different steady-state curves from various cell types and IPR subtypes, all showing the same fundamental bell shape). At low  $\text{Ca}^{2+}$  concentrations RyR exhibit a similar behaviour, in that an increase in  $\text{Ca}^{2+}$  concentration leads to a greater open probability of the RyR and thus CICR. At high  $\text{Ca}^{2+}$  concentrations the steady-state properties of the RyR are less clear, and there remains controversy over whether the RyR closes again at physiological  $\text{Ca}^{2+}$  concentrations, and what role such closure might play in excitation-contraction coupling [16, 47, 46, 58, 153].

The second way that CICR can arise is through a dynamic process, in which the activation of the IPR by  $\text{Ca}^{2+}$  is faster than its inactivation by  $\text{Ca}^{2+}$  leading to an initial large increase in  $\text{Ca}^{2+}$  release followed by a slower decline to a lower steady value [36, 48, 50, 66]. In this case, the CICR is a result of the differing time scales of IPR activation and inactivation. If CICR arises from this dynamic process, then it is largely independent of the shape of the steady-state open probability curve. In reality, IPR have both a bell-shaped steady-state curve as well as a time separation between  $\text{Ca}^{2+}$ -induced activation and  $\text{Ca}^{2+}$ -induced inactivation. It is thus not necessarily obvious which of these mechanisms underlies any particular experimental observation of CICR; most models, either deterministic or stochastic, incorporate aspects of both mechanisms [2, 33, 43, 120, 126, 137].

As a result of CICR,  $\text{Ca}^{2+}$  release through IPR and RyR is an autocatalytic, or positive feedback, process, similar in many aspects to the excitability seen in the membrane potential of a neuron [65]. In neurons, the positive feedback occurs via voltage-dependence of the  $\text{Na}^+$  channel, which causes a fast depolarisation of the cell. (Excitability of the  $\text{Na}^+$  channel arises from the fast activation and slow inactivation of the channel by the membrane potential [73].) Thus, standard excitable models, such as the FitzHugh-Nagumo model, have often been used in models of  $\text{Ca}^{2+}$  oscillations and waves [21, 127, 141, 142].

However, despite the similarities between the systems, models of  $\text{Ca}^{2+}$  dynamics differ in important ways from models of other excitable systems. We shall explore some of these differences in this review.

## 2 ODE models

If a cell is assumed to be well mixed, a typical equation for the  $\text{Ca}^{2+}$  concentration expresses simply the conservation of  $\text{Ca}^{2+}$ .

A simple example is shown in Fig. 4. There, the shaded area is the endoplasmic reticulum (ER), and there are five fluxes into or out of the cytoplasm. Two of those fluxes,  $J_{\text{in}}$  (a generic influx of  $\text{Ca}^{2+}$ , possibly through store-operated channels, agonist-operated channels, or voltage-dependent  $\text{Ca}^{2+}$  channels) and  $J_{\text{pm}}$  (the flux through the plasma membrane ATPase pumps), are across the plasma membrane, while the other three,  $J_{\text{RyR}}$  (the flux through RyR),  $J_{\text{IPR}}$  (the flux through IPR)

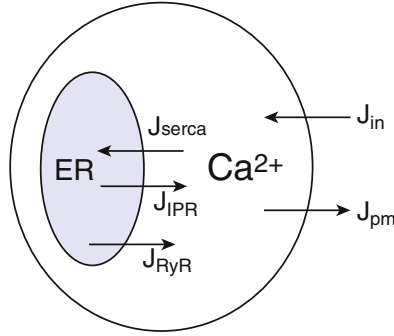


**Fig. 4** Schematic diagram of a simple spatially homogeneous  $\text{Ca}^{2+}$  dynamics model, with five fluxes. In this model,  $\text{Ca}^{2+}$  is pumped into the ER from the cytoplasm by SERCA pumps ( $J_{\text{serca}}$ ), is pumped out of the cell by plasma membrane ATPase pumps ( $J_{\text{pm}}$ ), enters the cytoplasm from the outside through some unspecified entry pathway ( $J_{\text{in}}$ ), and enters the cytoplasm from the ER through two channels, the IPR and the RyR

and  $J_{\text{serca}}$  (the flux through the SERCA pumps) are across the ER membrane. (For simplicity we ignore  $\text{Ca}^{2+}$  buffering for now. This is dealt with in detail in the next section.)

If we let  $c$  and  $c_e$  denote the  $\text{Ca}^{2+}$  concentration in the cytoplasm and ER, respectively, with respective volumes  $V$  and  $V_e$ , then conservation of  $\text{Ca}^{2+}$  gives

$$\frac{d}{dt}(cV) = J_{\text{in}} - J_{\text{pm}} + J_{\text{IPR}} + J_{\text{RyR}} - J_{\text{serca}}, \quad (2.1)$$

$$\frac{d}{dt}(c_e V_e) = -J_{\text{IPR}} - J_{\text{RyR}} + J_{\text{serca}}, \quad (2.2)$$

where each  $J$  is in units of moles per second.

As long as the volumes of the cytoplasm and ER remain constant, we can divide out the volumes to get

$$\frac{dc}{dt} = \frac{1}{V}(J_{\text{in}} - J_{\text{pm}} + J_{\text{IPR}} + J_{\text{RyR}} - J_{\text{serca}}), \quad (2.3)$$

$$\frac{dc_e}{dt} = -\frac{1}{V_e}(-J_{\text{IPR}} - J_{\text{RyR}} + J_{\text{serca}}). \quad (2.4)$$

In simple models like this it is usual to rescale all the fluxes, so that they have units of moles per time per cytoplasmic volume. Thus, we define, for example, a new  $\tilde{J}_{\text{in}} = J_{\text{in}}/V$ , and rewrite both equations in these new units.

If we do this, and then (for notational convenience) drop the tildes, we get

$$\frac{dc}{dt} = J_{\text{IPR}} + J_{\text{RyR}} - J_{\text{serca}} + J_{\text{in}} - J_{\text{pm}}, \quad (2.5)$$

$$\frac{dc_e}{dt} = \gamma(-J_{\text{IPR}} - J_{\text{RyR}} + J_{\text{serca}}), \quad (2.6)$$

where  $\gamma = \frac{V}{V_e}$ . The factor of  $\gamma$  appears since the flux of  $x$  moles from the cytoplasm to the ER causes a different change in concentration in each compartment, due to their different volumes. Each  $J$  is in units of moles per cytoplasmic volume per second.

Now one selects whichever model one wishes for each of the individual fluxes to complete the model construction. In general, each of these fluxes will involve other dynamic variables, which increases the total number of differential equations. Simpler models will have only two equations, more complex models typically have as many as eight, or even more.

We emphasise that, although this simple model omits a vast amount of the known complexity in  $\text{Ca}^{2+}$  signalling (such as microdomains, the influence of the mitochondria, and direct effects of the membrane potential), it is still (as we shall see) a useful tool for the study of the mechanisms underlying  $\text{Ca}^{2+}$  oscillations, in some conditions.

## 2.1 Calcium buffering

Calcium is heavily buffered in all cells, with at least 99% (and often more) of the available  $\text{Ca}^{2+}$  bound to large  $\text{Ca}^{2+}$ -binding proteins. For example, calsequestrin and calreticulin are major  $\text{Ca}^{2+}$  buffers in the ER and SR, while in the cytoplasm  $\text{Ca}^{2+}$  is bound to calbindin, calretinin and parvalbumin, among many others. Calcium pumps and exchangers and the plasma membrane itself are also major  $\text{Ca}^{2+}$  buffers. In essence, a free  $\text{Ca}^{2+}$  ion in solution in the cytoplasm cannot do much, or go far, before it is bound to something.

The basic chemical reaction for  $\text{Ca}^{2+}$  buffering can be represented by the reaction



where P is the buffering protein and B is buffered  $\text{Ca}^{2+}$ . Letting  $b$  denote the concentration of buffer with  $\text{Ca}^{2+}$  bound, and  $c$  the concentration of free  $\text{Ca}^{2+}$ , a simple model of  $\text{Ca}^{2+}$  buffering is

$$\frac{dc}{dt} = f(c) + k_-b - k_+c(b_t - b), \quad (2.8)$$

$$\frac{db}{dt} = -k_-b + k_+c(b_t - b), \quad (2.9)$$

where  $k_-$  is the rate constant for  $\text{Ca}^{2+}$  release from the buffer,  $k_+$  is the rate constant for  $\text{Ca}^{2+}$  uptake by the buffer,  $b_t$  is the total buffer concentration and  $f(c)$  denotes all the other reactions involving free  $\text{Ca}^{2+}$  (release from the  $\text{IP}_3$  receptors, reuptake by pumps, etc.). Note that, from conservation of buffer molecules,  $[\text{P}] + b = b_t$ .

If the buffer has fast kinetics, its effect on the intracellular  $\text{Ca}^{2+}$  dynamics can be analysed simply [147]. If  $k_-$  and  $k_+c_0$ , where  $c_0$  is some natural scale for the  $\text{Ca}^{2+}$  concentration (often around  $1 \mu\text{M}$ ), are large compared to the time constant of  $\text{Ca}^{2+}$  reaction (for example, the speed of release through the IPR or uptake by SERCA pumps), we take  $b$  to be in the quasi-steady state

$$k_-b - k_+c(b_t - b) = 0, \quad (2.10)$$

and so

$$b = \frac{b_t c}{K + c}, \quad (2.11)$$

where  $K = k_-/k_+$ . Adding (2.8) and (2.9), we find the “slow” equation

$$\frac{d}{dt}(c + b) = f(c), \quad (2.12)$$

which, after using (2.11) to eliminate  $b$ , becomes

$$\frac{dc}{dt} = \frac{f(c)}{1 + \theta(c)}, \quad (2.13)$$

where

$$\theta(c) = \frac{b_t K}{(K + c)^2}. \quad (2.14)$$

Note that we assume that  $b_t$  is a constant. Hence, fast  $\text{Ca}^{2+}$  buffering simply adds a  $\text{Ca}^{2+}$ -dependent scaling factor to all the fluxes.

If the buffer is not only fast, but also of low affinity, so that  $K \gg c$ , it follows that

$$\theta \approx \frac{b_t}{K}, \quad (2.15)$$

a constant. Such a constant, multiplying all the fluxes in the model, can be simply incorporated into the other rate constants, and ignored henceforth, with the proviso that all fluxes must be interpreted as effective fluxes, i.e., that portion of the actual flux that contributes to a change in free  $[\text{Ca}^{2+}]$ . Hence although it might appear at first glance that equation (2.5) ignores  $\text{Ca}^{2+}$  buffering, that is not the case. Rather, it is just assuming that  $\text{Ca}^{2+}$  buffering is fast and linear, and thus that all fluxes are effective fluxes.

There have been a number of studies of the effects of nonlinear buffers on the dynamics of  $\text{Ca}^{2+}$  oscillations (for example, see [52] or [42]), but these results are beyond the scope of this review. In general, the qualitative effects of nonlinear buffers are small, except in certain narrow parameter regimes. In this review we shall mostly just assume that buffering is fast and linear, and thus does not appear explicitly. An asymptotic analysis of  $\text{Ca}^{2+}$  buffering was performed by [121]; other important theoretical papers on  $\text{Ca}^{2+}$  buffering are [98, 100, 122, 123, 128, 141].

## 2.2 Modelling the calcium fluxes

In order to construct a specific realisation of (2.5) and (2.6), we need first to decide how to model each of the calcium fluxes in those equations. Since there is an enormous range of possible choices, we shall focus only on a few selected models.

### 2.2.1 IPR fluxes

Probably the most important, and the most difficult to model, fluxes are those through the IPR and RyR. IPR models have had a long and complicated history, starting from the earliest models of [33] and [55], through to the most recent models based on single-channel data [18, 118, 116]. Earlier models are reviewed in [126].

All these models share one crucial feature – that the steady-state open probability of the IPR is a bell-shaped function of  $[\text{Ca}^{2+}]$  (Fig. 5), as has been shown

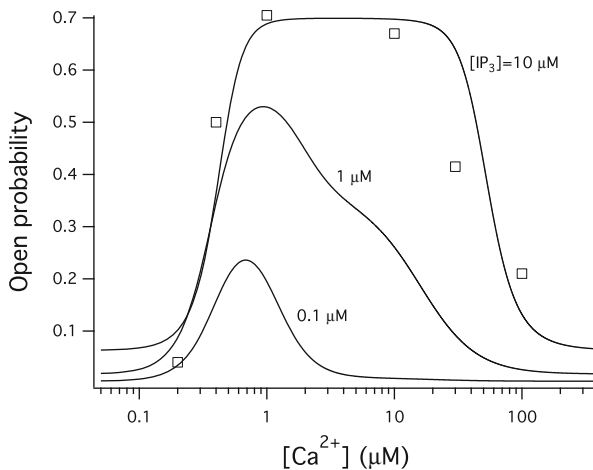


**Fig. 5** Open probability ( $P_o$ ) of the IPR as a function of  $\text{Ca}^{2+}$  is bell-shaped, increasing at lower  $[\text{Ca}^{2+}]$  and decreasing at higher  $[\text{Ca}^{2+}]$ . Open squares are data from type I IPR, measured at 10  $\mu\text{M}$   $[\text{IP}_3]$  [148], and the smooth curves are from the model of [18]



experimentally many times [50]. However, there are many different ways of attaining such a steady-state curve, and many different ways of modelling the dynamic features of the IPR.

In earlier models [33, 2, 125], the most important basic dynamic property of  $\text{IP}_3$  receptors is that they respond in a time-dependent manner to step changes of  $\text{Ca}^{2+}$  or  $\text{IP}_3$ . Thus, in response to a step increase of  $\text{IP}_3$  or  $\text{Ca}^{2+}$  the receptor open probability first increases to a peak and then declines to a lower plateau. This decline is called *adaptation* of the receptor, since the open probability adapts to a maintained  $\text{Ca}^{2+}$  or  $\text{IP}_3$  concentration. If a further step is applied on top of the first, the receptor responds with another peak, followed by a decline to a plateau. In this way the IPR responds to *changes* in  $[\text{Ca}^{2+}]$  or  $[\text{IP}_3]$ , rather than to absolute concentrations.

One popular model is one of the earliest, due to De Young and Keizer [33]. In this model, it is assumed that the  $\text{IP}_3$  receptor consists of three equivalent and independent subunits, all of which must be in a conducting state for there to be  $\text{Ca}^{2+}$  flux. Each subunit has an  $\text{IP}_3$  binding site, an activating  $\text{Ca}^{2+}$  binding site, and an inactivating  $\text{Ca}^{2+}$  binding site, each of which can be either occupied or unoccupied, and thus each subunit can be in one of eight states.

Simplification by Li and Rinzel [86] of this eight-state model led to the model

$$P_o = \left( \frac{pcr}{(p + K_1)(c + K_5)} \right)^3, \quad (2.16)$$

$$\tau_r(c, p) \frac{dr}{dt} = r_\infty(c, p) - r, \quad (2.17)$$

where  $P_o$  is the open probability,  $p$  is  $[\text{IP}_3]$ ,  $K_1$  and  $K_5$  are constants, and  $r$  is the fraction of receptors that have not been inactivated. The functions  $\tau_r$  and  $r_\infty$  are given in detail in [86]. Writing the model in this form emphasises the mathematical similarities with the model of the  $\text{Na}^+$  channel in the Hodgkin-Huxley model [65], thus highlighting their common feature of excitability.

A similar model, that appeared at the same time as the De Young and Keizer model, is due to Atri et al. [2] and takes a slightly simpler form. In the Atri model, the open probability of the IPR is assumed to take the form

$$P_o = k_f \left( \mu_0 + \frac{\mu_1 p}{k_\mu + p} \right) \left( b + \frac{(1-b)c}{k_1 + c} \right) r, \quad (2.18)$$

$$\tau \frac{dr}{dt} = \frac{k_2^2}{k_2^2 + c^2} - r. \quad (2.19)$$

Thus,  $P_o$  is an increasing function of the  $\text{IP}_3$  concentration, and, over fast time scales, an increasing function of  $c$  also. However, on the time scale set by  $\tau$ ,  $r$  acts as a  $\text{Ca}^{2+}$ -dependent inactivation variable, and causes  $\text{Ca}^{2+}$ -dependent and time-dependent inactivation of the receptor. (As in the Li-Rinzel model,  $r$  denotes the fraction of receptors that have not been inactivated by  $\text{Ca}^{2+}$ ). Overall, this model

gives a bell-shaped steady-state open probability curve, as seen experimentally, but has no satisfactory biophysical basis for the various terms.

Mathematical studies of  $\text{Ca}^{2+}$  dynamics have tended to use early IPR models, such as the ones described above. However, the most recent data have shown that the details of these early IPR models are not correct. We now know that the IPR exists in two (or possibly more) “modes” [18, 67, 93, 116, 118]. In one mode (sometimes called the Park mode) the receptor is mostly closed, while in the other mode (the Drive mode) the receptor is mostly open. Transitions between the two modes are controlled by  $[\text{Ca}^{2+}]$ ,  $[\text{IP}_3]$  and  $[\text{ATP}]$ , among other things, but transitions within each mode are independent of these ligands. Such modal behaviour cannot be reproduced by most early models, which have the incorrect Markov structure. In addition, the early models do not usually give the open-time and closed-time distributions (to choose two statistics in particular) that have been observed in the most recent single-channel data from nuclear patch clamp studies.

Nevertheless, although the details of the early models are incorrect, the fundamental IPR properties remain the same. For example, [18] has shown that fast  $\text{Ca}^{2+}$ -induced activation followed by slow  $\text{Ca}^{2+}$ -induced inactivation remain as crucial ingredients in these recent modal models.

For this reason, we shall focus here on mathematical studies of  $\text{Ca}^{2+}$  models based on older IPR models. When the newer generation of IPR models come to be incorporated into whole-cell models, the mathematical techniques (and dangers thereof) will remain the same.

## 2.2.2 RyR fluxes

The selection of RyR models is similarly complex. Some models [51] are based on simple and heuristic CICR, and fit data well, while a variety of other models, mostly designed for use in cardiac cell models [57, 56, 132, 151], incorporate multiple receptor states and stochastic behaviour. Because the literature on cardiac cells, skeletal muscle, RyR models and excitation-contraction coupling is so vast, we cannot even begin to do it justice in this review. Thus, we shall take the opposite approach and simply not discuss these areas at all (except in some restricted cases). The reviews of [8, 46] give excellent entries to the field, as do [7, 17, 16, 56, 115, 132, 145, 151].

## 2.2.3 Calcium pumps

Experimental data indicate that SERCA pumps transfer two  $\text{Ca}^{2+}$  ions across the ER/SR membrane per cycle [14, 89, 97, 138]. Thus, the most common way to model the  $\text{Ca}^{2+}$  flux,  $J_{\text{serca}}$ , due to SERCA pumps, is to use a simple Hill equation, with Hill coefficient of two. Thus,

$$J_{\text{serca}} = \frac{V_m c^2}{K_m^2 + c^2}.$$

The parameter  $K_m$  we know to be approximately  $0.27 \mu\text{M}$ , while  $V_m$ , which depends on the density of SERCA pumps, can vary substantially depending on the cell type.

It is worth noting that this equation for  $J_{\text{serca}}$  contains within it a host of simplifications. More detailed models of SERCA pumps [63, 77, 89, 138] involve multiple states, with the pump protein moving between these states to pick up  $\text{Ca}^{2+}$  ions on one side of the ER membrane and release them on the other. More accurate models of SERCA pumps would take these states into account, as well as keeping track of all the  $\text{Ca}^{2+}$  bound to the pump protein. ([73] gives an introductory discussion of a range of SERCA models, ranging from the simplest, to more complex versions.) Although such detailed models appear to cause little change in dynamic behaviour [63] one should keep in mind that the simplifications used to obtain  $J_{\text{serca}}$  (for example, quasi-steady-state approximations) are of the exact same type as those used to simplify  $\text{Ca}^{2+}$  models, as discussed in this review, and come with all the same caveats and potential for complications.

## 2.2.4 Calcium influx

Over recent years it has become clear that the influx of  $\text{Ca}^{2+}$  into the cell from outside is no simple matter [112, 117, 124, 131]. It is controlled by a variety of proteins that are themselves controlled by a variety of factors such as arachidonic acid, or the concentration of  $\text{Ca}^{2+}$  in the ER. For some of these influx pathways geometrical factors, such as the close apposition of the ER and the plasma membrane, play a significant role.

However, for the purposes of the discussion here, we can divide all  $\text{Ca}^{2+}$  influx pathways into three major types.

1. Voltage-dependent  $\text{Ca}^{2+}$  channels, or VDCCs [19]. These open in response to depolarisation of the cell membrane, and play a vital role in excitable cells such as skeletal and cardiac muscle, in some smooth muscle cells, in neuroendocrine cells, and in a variety of neuronal cell types.
2. Receptor-operated channels, or ROCs [70]. Some  $\text{Ca}^{2+}$  influx pathways open in response to agonist stimulation, often via the production of arachidonic acid. Thus,  $\text{Ca}^{2+}$  influx is usually modelled as an increasing function of agonist concentration. The exact mechanisms of this dependency are, in general, unknown, so detailed models of ROCs are not realistically possible at this stage.
3. Store-operated channels, or SOC [103]. Severe depletion of the ER causes the opening of  $\text{Ca}^{2+}$  channels in the cell membrane, via a process involving ORAI and STIM molecules. This is an important influx pathway under conditions of high prolonged agonist concentration, but will play little role in our analysis here.

## 2.3 Model classification

### 2.3.1 Open cell/Closed cell models

One common experimental technique is to remove  $\text{Ca}^{2+}$  from outside the cell, and observe how this affects the intracellular  $\text{Ca}^{2+}$  oscillations. In many cases the oscillations continue for a considerable time before finally running down (due to the progressive loss of  $\text{Ca}^{2+}$  from the cell), while in other cases the oscillations are terminated immediately. This has motivated the detailed study of the effects of  $\text{Ca}^{2+}$  entry on oscillatory properties.

To study the effects of  $\text{Ca}^{2+}$  entry, models are generally constructed in two different classes.

- Open cell models are those in which  $\text{Ca}^{2+}$  is allowed to enter and leave the cell freely across the plasma membrane. Thus, such models include  $\text{Ca}^{2+}$  influx pathways and plasma membrane  $\text{Ca}^{2+}$  pumps, and the total amount of  $\text{Ca}^{2+}$  in the cell is not conserved.
- Closed cell models are those in which all  $\text{Ca}^{2+}$  transport across the plasma membrane, both inward and outward, is blocked. Note that a closed cell model does not correspond exactly to the experimental situation of low external  $\text{Ca}^{2+}$  concentration, but will approximate the situation at the beginning of the experiment. It is possible experimentally to block the plasma membrane  $\text{Ca}^{2+}$  pumps also, using high concentrations of ions such as lanthanum, but these are more difficult experiments to perform and more difficult to interpret, due to the varied effects of lanthanum.

### 2.3.2 Class I/Class II models

The second way in which  $\text{Ca}^{2+}$  oscillation models are typically classified is with respect to the behaviour of  $\text{IP}_3$ . In some cell types,  $\text{Ca}^{2+}$  oscillations occur when  $\text{IP}_3$  concentration is constant, and such oscillations are believed to be caused by the intrinsic dynamics (i.e., the fast activation and slower inactivation by  $\text{Ca}^{2+}$ ) of the IPR [130]. Models of such oscillations are called Class I models. In other cell types,  $\text{Ca}^{2+}$  oscillations are necessarily accompanied by  $\text{IP}_3$  oscillations, and if those  $\text{IP}_3$  oscillations are blocked, so are the  $\text{Ca}^{2+}$  oscillations. In such cells, the feedback loops illustrated in Fig. 3 are an integral part of the oscillation mechanism. Such models are called Class II models. Models which partake both of Class I and Class II properties are called *hybrid* models [35]. Although, realistically, every cell type will have both Class I and Class II mechanisms to differing degrees, and thus should be modelled by a hybrid model, it is useful to make this distinction, and to study the behaviour of pure Class I and II models.

It is also important to note that  $\text{Ca}^{2+}$  oscillations can also be generated by the entry and exit of  $\text{Ca}^{2+}$  from the cell. Such oscillations cease immediately upon

removal of extracellular  $\text{Ca}^{2+}$ , and thus require an open-cell model. However, models of this type are neither Class I nor Class II. A simple example of this type of model is discussed in Section 5.3.

## 2.4 A simple example: the combined model

All these concepts, and the various types of models, can be simply illustrated by a single set of equations [35]. For convenience, we shall call this model the *combined* model, as it combines both Class I and Class II mechanisms in such a way that it is simple to switch from one class of model to the other.

As usual, we let  $c$  and  $c_e$  denote, respectively, the concentrations of  $\text{Ca}^{2+}$  in the cytoplasm and the ER, we let  $p$  denote the  $\text{IP}_3$  concentration, and we let  $r$  denote the fraction of IPR that have not been inactivated by  $\text{Ca}^{2+}$  (as in the Atri model described above).

$$\frac{dc}{dt} = J_{\text{IPR}} - J_{\text{serca}} + \delta(J_{\text{influx}} - J_{\text{pm}}), \quad (2.20)$$

$$\frac{dc_e}{dt} = \gamma(-J_{\text{IPR}} + J_{\text{serca}}), \quad (2.21)$$

$$\frac{dp}{dt} = \nu \left( 1 - \frac{\alpha k_4}{c + k_4} \right) - \beta p, \quad (2.22)$$

$$\frac{dr}{dt} = \frac{1}{\tau} \left( \frac{k_2^2}{k_2^2 + c^2} - r \right), \quad (2.23)$$

where

$$J_{\text{IPR}} = \left[ k_{\text{flux}} \left( \mu_0 + \frac{\mu_1 p}{k_\mu + p} \right) \left( b + \frac{V_1 c}{k_1 + c} \right) r \right] (c_e - c), \quad (2.24)$$

$$J_{\text{serca}} = \frac{V_e c}{K_e + c}, \quad (2.25)$$

$$J_{\text{pm}} = \frac{V_p c^2}{k_p^2 + c^2}, \quad (2.26)$$

$$J_{\text{influx}} = \alpha_1 + \alpha_2 \frac{\nu}{\beta}. \quad (2.27)$$

We note a number of things about this model.

- It uses the Atri model of the IPR [2], and the IPR flux is multiplied by the term  $c_e - c$ , so that it depends on the  $\text{Ca}^{2+}$  concentration gradient between the ER and

the cytoplasm. It could, just as easily, have used one of the other IPR models in the literature, and the results would, by and large, be qualitatively similar; our choice of the Atri model is purely for simplicity.

- The SERCA pumps are modelled by a Hill function, with Hill coefficient 1. This ignores cooperativity in the SERCA pumps, and thus is not the most accurate assumption that can be made, but it simplifies the analysis somewhat, and has little effect on the results we present here.
- The  $\text{IP}_3$  concentration,  $p$ , obeys its own differential equation, where the production of  $p$  can be  $\text{Ca}^{2+}$ -dependent, as long as  $\alpha \neq 0$ . However, if  $\alpha = 0$ , the equation for  $p$  essentially decouples. Hence,  $\alpha = 0$  corresponds to a Class I model.
- In the limit as  $\tau \rightarrow 0$ ,  $r$  becomes an algebraic function of  $c$ . Thus, the case  $\tau \rightarrow 0$  and  $\alpha \neq 0$  corresponds to a Class II model, in which any oscillations are governed by the interactions between  $c$  and  $p$ , not by the dynamics of the IPR.
- The parameter  $\delta$  is introduced so that the rate of  $\text{Ca}^{2+}$  transport across the plasma membrane can be easily controlled. In many cell types  $\delta$  is small compared to the time scales of  $\text{Ca}^{2+}$  transport and release through the IPR and SERCA pumps.
- The parameter  $\nu$  corresponds to the maximal rate of  $\text{IP}_3$  production, and is a surrogate for the agonist concentration; as the agonist concentration increases, both the rate of production of  $\text{IP}_3$  and the rate of  $\text{Ca}^{2+}$  influx from the outside increases. Thus, in this model,  $\text{Ca}^{2+}$  influx is via receptor-operated channels.  $J_{\text{influx}}$  is a linear function of agonist concentration, an expression which has no biophysical basis, but is merely the simplest possible way to make  $\text{Ca}^{2+}$  influx increase with agonist. As usual with models like this, many of the terms are suggestive of what we believe are the actual mechanisms, but should not be interpreted too literally.

A useful approach, that accentuates the difference between open cell models and closed cell models, is to express the model in terms of a new variable,  $c_t = c + c_e/\gamma$ , where  $\gamma$  is the ratio of cytoplasmic to ER volume, as defined after eqn. (2.6). Thus,  $c_t$  is the total number of moles of  $\text{Ca}^{2+}$  in the cell, divided by the cytoplasmic volume, and is a measure of the  $\text{Ca}^{2+}$  load of the cell, i.e., how much  $\text{Ca}^{2+}$  the cell contains. Using this new variable the first two model equations become

$$\frac{dc}{dt} = J_{\text{IPR}} - J_{\text{serca}} + \delta(J_{\text{influx}} - J_{\text{pm}}), \quad (2.28)$$

$$\frac{dc_t}{dt} = \delta(J_{\text{influx}} - J_{\text{pm}}). \quad (2.29)$$

It is now clear that, as  $\delta$  becomes smaller,  $c_t$  becomes a slower variable than  $c$ , and in the limit of  $\delta = 0$  we obtain a closed cell model.

Hence, by varying  $\alpha$ ,  $\delta$  and  $\tau$  we can use this single set of equations to illustrate both open and closed cell models, as well as Class I and Class II models.

### 3 Bifurcation structure of ODE models

A natural first step towards understanding the dynamics of models such as the combined model (i.e., equations (2.20)–(2.23)) is to construct a bifurcation diagram; this allows us to locate parameter regimes in which behaviour of interest, such as calcium oscillations, can occur. For most models, there are many possible choices of bifurcation parameter, but it is common to choose as the main bifurcation parameter a quantity that corresponds to something that is relatively easy to manipulate experimentally. Doing so makes it easier to compare model output to experimental results, and thus to validate the model or use model predictions to inform experiments. For instance, in the combined model, we can choose  $\nu$  as the primary bifurcation parameter;  $\nu$  corresponds to the maximal rate of  $\text{IP}_3$  production, which is relatively easy to modify in an experiment since it is an increasing function of the level of agonist applied to the cell.

Fig 6A shows a partial bifurcation diagram for the combined model, for the choice  $\alpha = 1$ ,  $\tau = 2$  (i.e., a hybrid version of the model) and other parameters as specified in Table 1 in the Appendix. Time series and phase portraits for two choices of  $\nu$  are shown in the other panels. This bifurcation diagram is typical of many models of intracellular calcium dynamics, in the sense that we see no oscillations of  $[\text{Ca}^{2+}]$  for sufficiently small or sufficiently large  $\nu$ , but there is a region of intermediate parameter values (between the points labelled  $\text{HB}_1$  and  $\text{HB}_2$ ) in which there is a variety of different types of oscillation. This is what is seen experimentally; at low agonist concentrations, there is not enough  $\text{IP}_3$  to open the IPR, while at high agonist concentration, there is so much  $\text{IP}_3$  in the cell, and such a high resting  $[\text{Ca}^{2+}]$ , that the IPR is again kept shut (remember that the steady-state open probability curve of the IPR is bell-shaped, and so the IPR is closed at both low and high  $[\text{Ca}^{2+}]$ ).

One feature common to both the time series shown is that there are time intervals in which there is very rapid increase or decrease of calcium concentration interspersed with intervals of much slower change. These are typical solutions for models with more than one time scale; in the case of the combined model, this results in part from the choice  $\delta = 0.01$ , which causes the variable  $c_t$  to evolve much more slowly than the variable  $c$ , at least for certain choices of the bifurcation parameter,  $\nu$ , and in certain regions of the phase space. Methods for the analysis of mathematical models with multiple time scales are well developed in general, although only recently applied in a systematic way to models of calcium dynamics; these methods are discussed further in section 3.1. For now, we note only that the oscillation shown in panels B and C of Fig 6 is a *relaxation oscillation*, while that shown in panels D and E is a *mixed mode oscillation*, and has a number of small, subthreshold oscillations occurring between each pair of large spikes in calcium concentration. Note that the subthreshold oscillations in panel D are of very small amplitude, and are essentially invisible on the scale of the main panel. However, the presence of these tiny oscillations can have a marked effect on the observed dynamics, as will be discussed further in section 3.2. At values of  $\nu$  close to  $\text{HB}_2$ , it

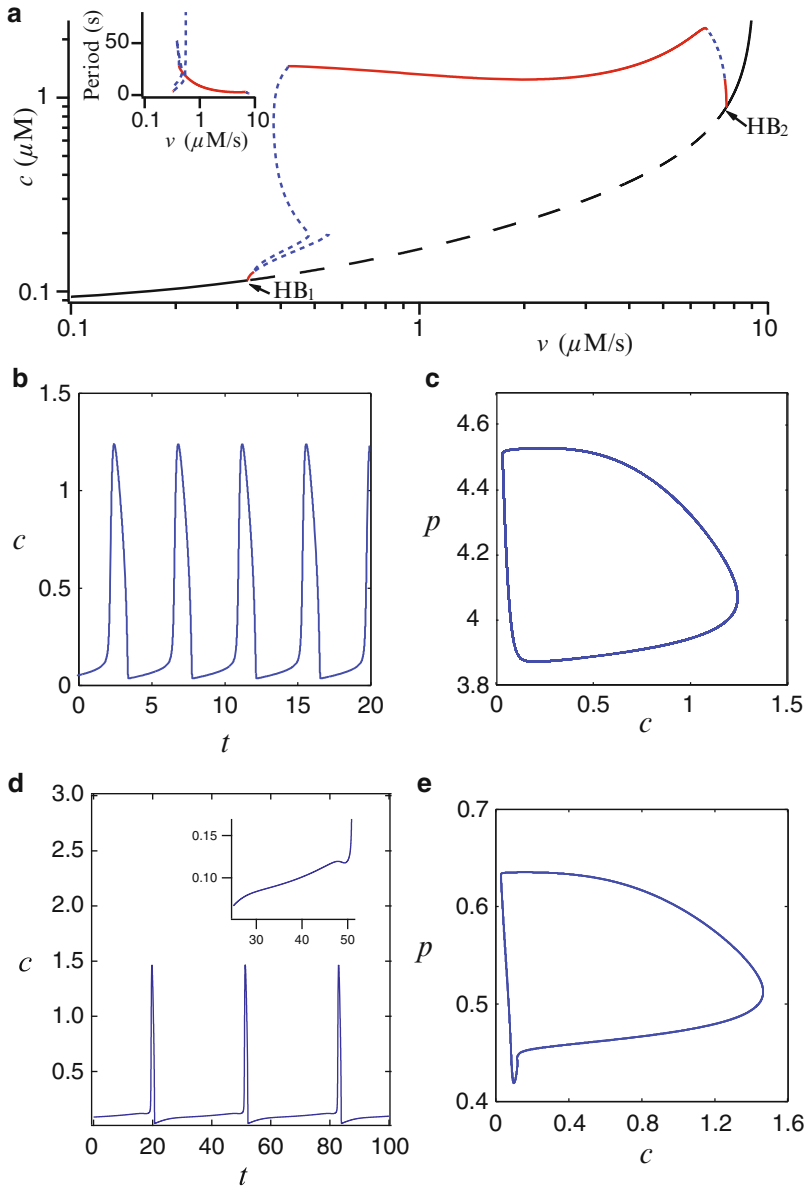


**Fig. 6** Partial bifurcation diagram and some time series and phase portraits for equations (2.20)–(2.27), with  $\alpha = 1$ ,  $\tau = 2$  and other parameter values as in Table 1. Panel A shows the bifurcation diagram, plotting the cytosolic calcium concentration,  $c$ , versus the maximal rate of  $\text{IP}_3$  formation,  $\nu$ . The black curve shows the position of the steady state solution (dashed curve when it is unstable, solid curve when it is stable). The red and blue curves indicate the maximum amplitudes of stable and unstable periodic orbits, resp. Hopf bifurcations are labelled HB. The inset shows the period of the branches of periodic orbit plotted in the main panel. Panels B and D show time series for  $c$  for the attracting periodic solutions that occur at  $\nu = 2.0$  and  $\nu = 0.4$ , resp., with the insert to panel D showing an enlargement of part of the time series. Panels C and E show the same solutions as in B and D, resp., projected onto the  $c$ - $p$  plane



is also possible to see attracting quasiperiodic oscillations, a feature quite commonly seen in calcium models. Further detail about the bifurcations associated with this and related models is contained in [35, 61] and [62].

Fig. 7A shows an analogous bifurcation diagram for the Class II version of the same model, i.e., with  $\alpha = 1$  and in the limit  $\tau \rightarrow 0$ . As can be seen, the range of  $\nu$  values for which oscillations occur is much smaller than for the hybrid model, and evidence in the time series for the existence of different time scales

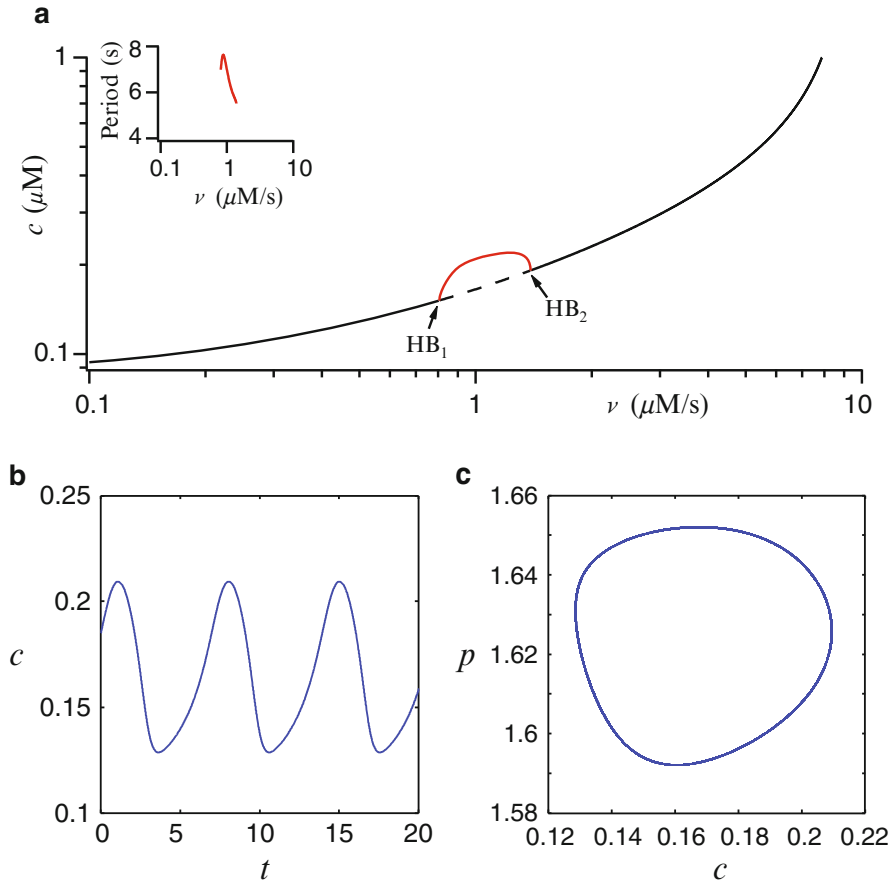


**Fig. 7** Partial bifurcation diagram and a corresponding time series and phase portrait for the combined model (equations (2.20)–(2.23)), with  $\alpha = 1$  and in the limit  $\tau \rightarrow 0$ , and with other parameter values as in Table 1. Panel A shows the bifurcation diagram, plotting the cytosolic calcium concentration,  $c$ , versus the maximal rate of  $\text{IP}_3$  formation,  $\nu$ . The inset shows the period of the branch of periodic orbits. Panel B shows a time series for  $c$ , for the attracting periodic solution that occurs at  $\nu = 1.0$ , and panel C shows the same solution projected onto the  $c$ - $p$  plane. Line styles and labels are as in Fig 6

is less pronounced. Similar time series (although with differing amplitudes of the oscillations) occur for all values of  $\nu$  for which there are oscillations.

Note that Fig 6A is an incomplete bifurcation diagram for the associated model; just the primary branches of periodic orbits are shown, and there are a number of bifurcations along these branches that have not been identified here (e.g., at each place where the stability of a periodic orbit branch changes). While a detailed knowledge of the bifurcation structure of a model may be of interest from a mathematical point of view, the details are frequently irrelevant from the point of view of understanding the underlying physiology. Data from typical experiments might consist of noisy time series of  $[\text{Ca}^{2+}]$  (or possibly both  $[\text{Ca}^{2+}]$  and  $[\text{IP}_3]$ ), from which an approximate amplitude and frequency of the oscillation can be extracted, but these may not be able to be directly compared with predictions from the model, due to the large number of unknown parameters in the model. Furthermore, unstable solutions will not be directly observed, and experimental time series may not have enough precision or length to resolve other details, such as subthreshold oscillations. We note, however, that an understanding of the mathematical details of model dynamics, including unstable solutions, sometimes provides crucial insight into physiological mechanisms that may underlie experimental observations; an example of such a case is discussed in section 3.2.

### 3.1 *Fast-slow reductions*

ODE models of calcium dynamics frequently exhibit behaviour indicative of the presence of different time scales in the problem, as discussed above, and a variety of techniques that exploit the time scale separation may be helpful in the analysis of these models. A first step in the process is identification of the time scales present in the model. Sometimes, an understanding of the physiology underlying the model assists this process. For instance, in many situations, the variation of the total calcium ( $c_t$ ) in a cell is known to be slow relative to variations in cytoplasmic or ER calcium concentrations (this was discussed above in the context of the combined model) and  $c_t$  can then be designated as a slow variable. There are good physiological reasons for this; as discussed in Section 1.1, cells expend a great deal of energy keeping cytoplasmic  $[\text{Ca}^{2+}]$  low, against a very large  $[\text{Ca}^{2+}]$  gradient. It is thus desirable for cells to restrict severely the ability for  $\text{Ca}^{2+}$  to cross the cell membrane. Hence, background  $\text{Ca}^{2+}$  influx into cells tends to be very slow, to be matched by an equally slow background  $\text{Ca}^{2+}$  removal from the cell.

However, beyond the designation of total calcium as a slow variable, the situation can be quite complicated: there may be more than one slow variable or more than two time scales, the relative speed of evolution of the variables may change within the phase space, and intuition based on physiological considerations may be misleading.

From a mathematical point of view, an approach that is frequently helpful is to non-dimensionalise the model equations, then group variables according to

their relative speed of evolution in the non-dimensional version of the model. For instance, as discussed in [62], a non-dimensional form of equations (2.22), (2.23), (2.28) and (2.29) can be obtained by introducing new dimensionless variables,  $(C, C_t, P, t_1)$  with

$$c = Q_c \cdot C, \quad c_t = Q_c \cdot C_t, \quad p = Q_p \cdot P, \quad t = T \cdot t_1,$$

where  $Q_c = 1 \mu M$  and  $Q_p = 10 \mu M$  are typical concentration scales for calcium and  $IP_3$ , resp., and  $T = Q_c/(\delta V_p) = 100/24$  s is a typical time scale for the  $c_t$  dynamics. (Note that the variable  $r$  was already dimensionless in the original model.) This then leads to rescaled evolution equations:

$$\begin{aligned} \delta \frac{dC}{dt_1} &= \bar{J}_{\text{release}} - \bar{J}_{\text{serca}} + \delta(\bar{J}_{\text{in}} - \bar{J}_{\text{pm}}), \\ \frac{dC_t}{dt_1} &= \bar{J}_{\text{in}} - \bar{J}_{\text{pm}}, \\ \frac{dr}{dt_1} &= \frac{1}{\hat{\tau}} \left( \frac{k_2^2}{k_2^2 + Q_c^2 C^2} - r \right), \\ \frac{dP}{dt_1} &= \hat{\nu} \left( 1 - \frac{k_4 \alpha}{k_4 + Q_c C} \right) - \hat{\beta} P, \end{aligned} \tag{2.30}$$

with dimensionless parameters

$$\hat{\tau} = \frac{\delta V_p}{Q_c} \tau, \quad \hat{\nu} = \frac{Q_c}{Q_p} \frac{\nu}{\delta V_p}, \quad \hat{\beta} = \frac{Q_c}{\delta V_p} \beta, \tag{2.31}$$

and corresponding dimensionless versions of the fluxes,  $\bar{J}_{\text{release}}$ ,  $\bar{J}_{\text{serca}}$ ,  $\bar{J}_{\text{pm}}$  and  $\bar{J}_{\text{in}}$ . With the choice of parameters values given in Table 1, and for  $\nu$  values corresponding to oscillatory solutions, we then find that the speeds of evolution for the variables are  $O(10^2)$  for  $C$ ,  $O(1)$  for  $C_t$  and  $P$ , and order  $O(1/\hat{\tau})$  for  $r$ . Thus, if  $\hat{\tau}$  is  $O(1)$ , this system has one fast variable and three slow variables, while if  $\hat{\tau}$  is  $O(\delta)$ , there are two fast variables and two slow variables.

A common next step in the analysis of certain classes of model is to remove fast variables using a quasi-steady state (QSS) approximation. The idea is that certain variables may evolve so fast that their evolution equations can be replaced by algebraic equations, thereby reducing the dimension of the model. For instance, in equations (2.30), if  $\hat{\tau}$  is small enough (e.g.,  $O(10^{-3})$  or smaller), then  $r$  can be regarded as the fastest variable of the model, and we might assume that  $dr/dt_1 \approx 0$  so that

$$r \approx \frac{k_2^2}{k_2^2 + Q_c^2 C^2}.$$

The QSS approximation replaces  $r$  in the model by its QSS value,  $r_\infty(C)$ :

$$r_\infty \equiv \frac{k_2^2}{k_2^2 + Q_c^2 C^2}.$$

The model then reduces to three differential equations, and becomes a Class II version of the model as discussed in section 2.4.

Although appealing from a modelling perspective, use of a QSS approximation can lead to difficulties. As discussed in [157], QSS reduction can remove a Hopf bifurcation from the dynamics or change the position or criticality of a Hopf bifurcation. In such cases, the occurrence and/or nature of oscillations in the reduced model may be significantly different to that for the original model, usually an undesirable outcome. Further work on the effect of QSS reduction is underway, but early results [157] suggest that singular Hopf bifurcations [13] (in which both fast and slow variables are involved in the bifurcation, and which are common in models of biophysical systems) may be relatively unaffected by QSS reduction.

A different reduction technique that has had some success in explaining the dynamics of calcium models involves effectively removing one of the slow variables by treating it as a parameter. This method was pioneered by Rinzel [108] in his classic study of bursting electrical oscillations in pancreatic beta cells, and has since been widely used in the study of a range of oscillating biophysical models. The idea is that characteristics of an attracting solution occurring at a particular value of the genuine bifurcation parameter can be understood by comparing it with the bifurcation diagram obtained by fixing the genuine bifurcation parameter but using the slowest variable as a parameter.

For instance, for the Class II version of the combined model expressed in  $(c, c_t, p)$  coordinates, i.e., equations (2.22), (2.28) and (2.29) with  $\alpha = 1$  and  $r(c) = \frac{k_2^2}{k_2^2 + c^2}$ , the variable  $c_t$  is slowest so long as  $\delta$  is sufficiently small. One can then remove the  $dc_t/dt$  equation and treat  $c_t$  as a constant where it appears elsewhere in the model, then construct a bifurcation diagram using  $c_t$  as the bifurcation parameter. For the choice  $\nu = 1.0$ , this method results in the bifurcation diagram shown in black in Fig 8. After superimposing on this bifurcation diagram the attracting orbit of the full problem, with  $c_t$  allowed to vary but with  $\nu$  still fixed at the same value, and with  $\delta = 0.0001$ , it can be seen that the orbit (shown in red in Fig 8) moves slowly near the stable branches of the bifurcation diagram, in a direction determined by the true value of  $dc_t/dt$ , and makes fast jumps between branches when it reaches the end of a stable section of the bifurcation diagram. In this way, the fast-slow nature of the orbit of the original problem with  $\delta = 0.0001$  can be ‘understood’ in terms of the bifurcation diagram of the system obtained by ‘freezing’ the slow variable  $c_t$ . By varying the value of the fixed (genuine) bifurcation parameter, one can then explain transitions between different types of orbit in the full system.

There are a number of potential difficulties with the use of this ‘frozen’ system approach. First of all, it presumes that a single globally valid slowest variable can be identified; in reality, variables may have different relative speeds of evolution in

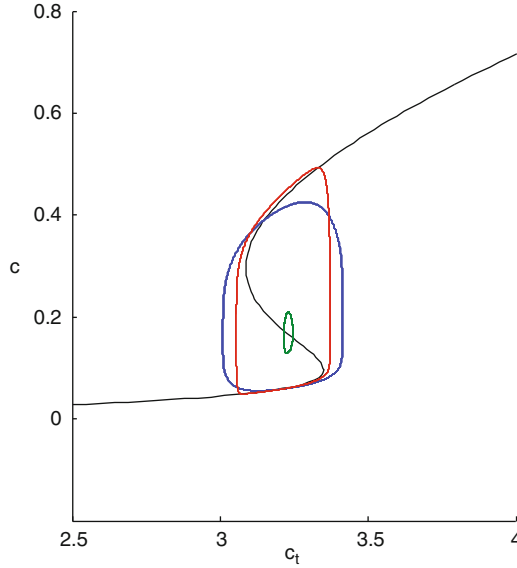


**Fig. 8** Bifurcation diagram of the ‘frozen’ Class II combined model, equations (2.22) and (2.28) with  $r(c) = \frac{k_2^2}{k_2^2 + c^2}$  and  $c_t$  treated as the bifurcation parameter. Parameter values are  $\nu = 1.0$ ,  $\alpha = 1$  and other constants as in Table 1. The black curve indicates steady states of the frozen system; the upper and lower branches are stable, the middle branch is unstable. The red (resp. blue and green) curve shows a solution of the full Class II system for  $\delta = 0.0001$  (resp. 0.001 and 0.01)

different parts of the phase space and at different values of the bifurcation parameter. Even if a slowest variable is identifiable, it may not be sufficiently slow for the method to be useful. For instance, Fig 8 shows orbits of the Class II combined model for the choices  $\delta = 0.01, 0.001$  and  $0.0001$ . Without a proper time scale analysis, it is not known in advance how small  $\delta$  needs to be for the ‘frozen’ system approach to be useful, but it is apparent from Fig 8 that  $\delta = 0.01$  is not small enough (the orbit with this value of  $\delta$  does not follow branches of the frozen bifurcation diagram) and that  $\delta = 0.001$  is marginal.

Second, many systems have more than one variable evolving on the slowest time scale; while it is possible to adapt the method to the case of two slow variables, the method rapidly becomes cumbersome. Third, this method may not give accurate information about the regions of transition from fast to slow sections of an orbit, which occur when the distinction between ‘fast’ and ‘slow’ variables is lost; these regions are often highly significant for distinguishing between different mechanisms in the dynamics (for instance, the difference between the relaxation oscillations and mixed mode oscillations shown in Fig. 6 occurs precisely at the point where the oscillations change from fast to slow evolution, and these differences are crucial for understanding some phenomena (see section 3.2)). Finally, limited information is provided by the method about the robustness of orbits to changes in the genuine bifurcation parameter.

A more rigorous approach involves the use of geometric singular perturbation theory (GSPT). The idea is to define one or more small parameters in the model. By regarding the model system as a perturbation from a limiting case in which the small parameter(s) tend to zero, it may be possible to extract useful information about the mechanisms underlying complicated dynamics in the original model. For instance, for system (2.30) in the case that  $\hat{\tau}$  is  $O(\delta)$ , we can introduce a small singular perturbation parameter  $\epsilon$ , and rewrite the model as

$$\begin{aligned}\epsilon \frac{dC}{dt_1} &= \bar{J}_{\text{release}} - \bar{J}_{\text{serca}} + \delta(\bar{J}_{\text{in}} - \bar{J}_{\text{pm}}) \\ \frac{dC_t}{dt_1} &= \bar{J}_{\text{in}} - \bar{J}_{\text{pm}} \\ \frac{dr}{dt_1} &= \frac{1}{\hat{\tau}} \left( \frac{k_2^2}{k_2^2 + Q_c^2 C^2} - r \right) \\ \frac{dP}{dt_1} &= \hat{v} \left( 1 - \frac{k_4 \alpha}{k_4 + Q_c C} \right) - \hat{\beta} P,\end{aligned}\tag{2.32}$$

As  $\epsilon \rightarrow 0$ , system (2.32) tends to a singular limit, usually called the *reduced system*. We can regard equations (2.30) as a perturbation of the singular limit, resulting from the choice  $\epsilon = 0.01 (= \delta)$  in equations (2.32). Alternatively, one can rewrite these equations using a fast time scale,  $t = t_1/\epsilon$ , which yields

$$\begin{aligned}\frac{dC}{dt} &= \bar{J}_{\text{release}} - \bar{J}_{\text{serca}} + \delta(\bar{J}_{\text{in}} - \bar{J}_{\text{pm}}) \\ \frac{dC_t}{dt} &= \epsilon \bar{J}_{\text{in}} - \bar{J}_{\text{pm}} \\ \frac{dr}{dt} &= \epsilon \frac{1}{\hat{\tau}} \left( \frac{k_2^2}{k_2^2 + Q_c^2 C^2} - r \right) \\ \frac{dP}{dt} &= \epsilon \hat{v} \left( 1 - \frac{k_4 \alpha}{k_4 + Q_c C} \right) - \hat{\beta} P,\end{aligned}\tag{2.33}$$

Equations (2.32) and (2.33) are equivalent for  $\epsilon \neq 0$ , but taking the limit as  $\epsilon \rightarrow 0$  of equations (2.33) produce a different singular system, known as the *fast subsystem*.

In the case that a model has two well-separated time scales, GSPT allows one to make predictions about the nature of oscillations occurring in the model, based on knowledge of the dynamics of the reduced system and the fast subsystem. The idea is to construct a singular periodic orbit consisting of alternating fast and slow segments; fast segments are solutions to the fast subsystem and slow segments are solutions of the reduced system. In the simplest cases (including the case where there is just one slow variable) a singular periodic orbit perturbs in a straightforward way when  $\epsilon \neq 0$  to produce a relaxation oscillation (RO) in the full system, with the corresponding time series consisting of sections of slow change interspersed with

sharp transitions as shown in Fig 6B. In other cases, the singular periodic orbit may perturb to a more complicated orbit such as a mixed mode oscillation (MMO), where the transition from slow to fast segments is via a series of subthreshold oscillations as shown in Fig 6D. The pattern of subthreshold oscillations within an MMO can be quite complicated but can often be predicted using GSPT [34]. A detailed study of the utility of GSPT for the analysis of a variety of different models of intracellular calcium dynamics is contained in [62].

An advantage of the GSPT approach is that the reduced system and the fast subsystem are both effectively of lower dimension than the full system, and so their analysis can be more straightforward than analysis of the full system directly. On the other hand, while GSPT can result in mathematically rigorous results accompanied by appropriate caveats about the regimes of validity of the results, this is not always useful in terms of understanding the dynamics of a model. A common problem is the lack of clear separation between time scales in the model. For instance, in equations (2.30), if  $\hat{\tau}$  is  $O(10^{-1})$  then the  $r$  variable is neither as fast as  $C$  nor as slow as  $C_t$  and  $P$ , and there is not enough of a separation between the speeds of evolution of  $r$  and the other variables to define a new intermediate time scale. In such cases, the model might be regarded as being a large perturbation of a singular limit, but then predictions based on a singular limit may be unhelpful. Even if there is clear separation between time scales in a model, there may be more than two time scales present, a situation about which there is little theory.

Some discussion of these kinds of difficulties in the context of calcium models is contained in [62]. One pragmatic approach is to consider a variety of different singular limits. For example to understand the dynamics of equations (2.30) in the case that  $r$  is intermediate in speed, one might look at two different limiting cases: one with two fast and two slow variables (with  $r$  treated as a fast variable) and the other with one fast and three slow variables (with  $r$  treated as a slow variable). One or other of these limiting cases might provide insight into the dynamics of the model, even if neither is close enough to the original model for predictions to be mathematically justified.

One final comment is in order about the use of singular limits in the analysis of calcium models; care is necessary in the identification and analysis of singular limits if misleading results are to be avoided. For instance, the closed cell version of the combined model arises naturally by letting the variable  $c_t$  get slower and slower. It is tempting therefore to regard the closed cell model as a singular limit (fast subsystem) of the open cell model, and, by analogy with the procedure followed in GSPT, to assume that the dynamics of the open cell model will be a smooth perturbation of the dynamics of the closed cell model. While some features of the dynamics do perturb in this simple manner, there is a trap: the dynamics of the limit system need not be the same as the limit of the dynamics of the full system. For example, a Hopf bifurcation may be subcritical in the fast subsystem but supercritical in the full system, *no matter how close the full system is to the limiting case*. This issue is discussed in more detail in [157]. A second reason for care in using the closed cell version of the combined model is implicit in the time scale analysis discussed above: in the open cell model,  $c_t$  appears to evolve on the

same time scale as  $p$  (and, possibly,  $r$ ) in the regime of interest, and so a singular limit in which the speed of evolution of  $c_t$  alone (not  $p$  or  $r$ ) tends to zero may not be helpful.

### 3.2 Pulse experiments and GSPT

An open question for many cell types is whether  $\text{Ca}^{2+}$  oscillations are principally due to Class I mechanisms (and occur when  $\text{IP}_3$  concentration is constant), or result from Class II mechanisms (being caused by the intrinsic dynamics of the IPR). One might be tempted to think that, since it is now possible to measure  $[\text{IP}_3]$  and  $[\text{Ca}^{2+}]$  simultaneously in some cell types [134], this question is easily answered. However, this would not be true. For one thing, these are very difficult experiments to perform, particularly in real cells as opposed to cell lines. Thus, there are still few such measurements in the literature. Secondly, even when one measures  $[\text{IP}_3]$  and  $[\text{Ca}^{2+}]$  simultaneously not all such questions are immediately answered. For instance, in some cell types, the relative timings of the peak  $[\text{IP}_3]$  and  $[\text{Ca}^{2+}]$  seem to indicate that a Class I mechanism is required, even though oscillations in  $[\text{IP}_3]$  are observed. In such cases, a peak of  $[\text{IP}_3]$  will naturally follow a peak in  $[\text{Ca}^{2+}]$  (as  $\text{Ca}^{2+}$  stimulates the production of  $\text{IP}_3$ ) but is not actually necessary for the oscillatory behaviour. For these reasons, it is important to develop additional experimental methods that can be used to distinguish between Class I and Class II mechanisms.

It was proposed in [130] that a simple experiment, involving applying a single exogenous pulse of  $\text{IP}_3$  to a cell, could be used to determine which type of mechanism was predominant in that cell. The proposal was based on the observation that Class I and Class II models typically respond to a pulse of  $\text{IP}_3$  in different ways. Specifically, after a pulse of  $\text{IP}_3$ , a Class I model will typically respond with a temporary increase in oscillation frequency while a Class II model will respond with a phase lag, with the next peak in calcium concentration occurring after a delay.

Fig. 9 shows some responses of the rescaled combined model given by equations (2.32) to a pulse of  $\text{IP}_3$ . As in [35] and [61], we model the pulsing process by adding

$$S(t_1) = \hat{M}H(t_1 - t_0)H(t_0 + \Delta - t_1) \quad (2.34)$$

to the right-hand side of the equation for  $P$  in the combined model, where  $\hat{M}$  denotes the pulse magnitude and  $H$  is the Heaviside function

$$H(x) = \begin{cases} 0 & \text{if } x < 0, \\ 1 & \text{if } x \geq 0. \end{cases}$$



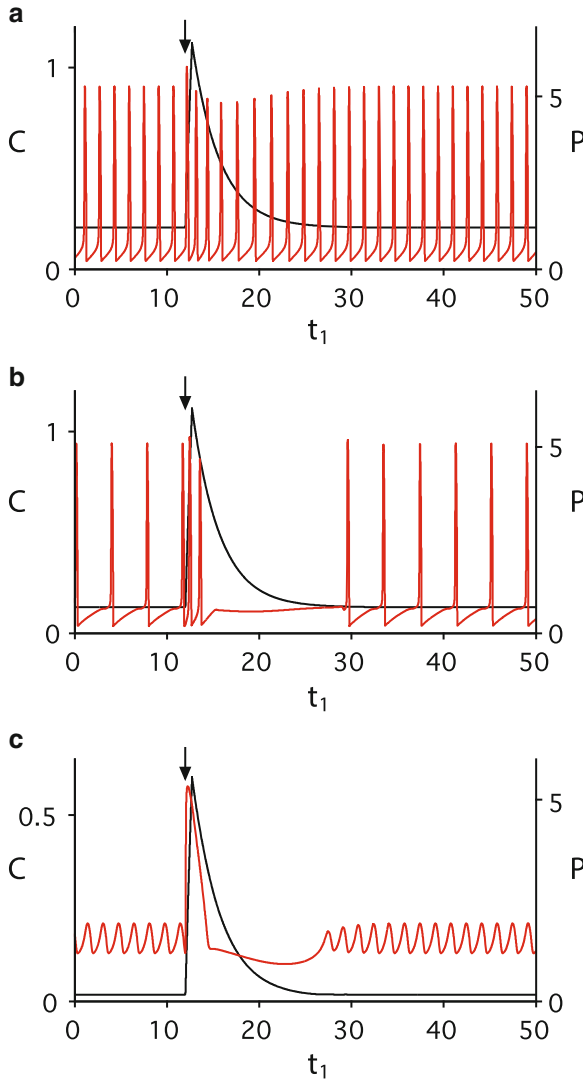


**Fig. 9** Responses of equations (2.32) with  $\epsilon = 0.01$  to IP<sub>3</sub> pulses. The IP<sub>3</sub> pulse is applied at the time indicated by the arrow, with the explicit form of the pulse given by equation (2.34) with  $\hat{M} = 8.33\hat{3}$ ,  $t_0 = 12$  and  $\Delta = 0.72$ , assuming that any transients have died out before the time trace is started. Each panel shows the time series of the concentrations  $C$  of calcium (red curve) and  $P$  of IP<sub>3</sub> (black curve). A. Class I:  $\alpha = 0$ ,  $\hat{\tau} = 0.48$  ( $\tau = 2s$ ) for  $\hat{\nu} = 0.40$  ( $\nu = 0.96$ ) and other parameter values as in Table 1. B. Class I: as in panel A except with  $\hat{\nu} = 0.233$  ( $\nu = 0.56$ ). C. Class II:  $\alpha = 1$ ,  $\hat{\tau} = 0$  ( $\tau = 0$ ) for  $\hat{\nu} = 0.417$  ( $\nu = 1.00$ ). Figure modified from [35]

Panel A shows the Class I model response when  $\hat{\nu} = 0.40$  and panel C shows the Class II model response when  $\hat{\nu} = 0.417$ . In both cases, the response is the typical case as described above. However, it turns out that there are situations in

which a Class I model responds like a Class II model, with a small number of faster oscillations followed by a long quiescent period before oscillations resume. Panel B of Fig. 9 shows this type of response for the Class I version of the combined model when  $\hat{\nu} = 0.233$ . The possibility of this anomalous type of response makes interpretation of experimental data ambiguous.

Attempts to understand the anomalous response of some Class I models began in [35], which considered pulse responses for the combined model of section 2.4. The analysis started with the assumption that there was one slow variable in the model,  $c_t$ , and used ideas based on the “frozen system” approach, discussed above, to explain the observed dynamics, but the explanation was somewhat ad hoc. The model was re-examined in [61], where it was argued that a comprehensive explanation of the phenomenon required methods from GSPT, and, in particular, that it was necessary to treat the Class I version of the model as a system with three slow variables.

More precisely, [61] worked with the non-dimensionalised Class I combined model given by equations (2.32) with  $\alpha = 0$  and  $\hat{\tau} = 0.48$ , and constructed singular periodic orbits by combining information from the reduced system and the fast subsystem, as described in section 3.1. Specifically, taking the limit  $\epsilon \rightarrow 0$  of equations (2.32) yields the reduced system, in which the variables evolve on a three-dimensional surface (the *critical manifold*) defined by setting the right-hand side of the  $dC/dt$  equation equal to zero. The critical manifold is plotted in Fig. 10 relative to the  $C$ ,  $C_t$  and  $r$  coordinates for the case  $\hat{\nu} = 0.317$  and with fixed  $P = 0.95$ . As can be seen, the critical manifold has two folds relative to the  $C$  coordinate. These folds are denoted by blue curves in Fig. 10 and correspond to two-dimensional subsets of the three-dimensional critical manifold in the full four-dimensional phase space. A typical singular orbit of the Class I Atri model then might start on the upper branch of the critical manifold (labelled  $S_a^+$  in Fig. 10), move (slowly) towards the

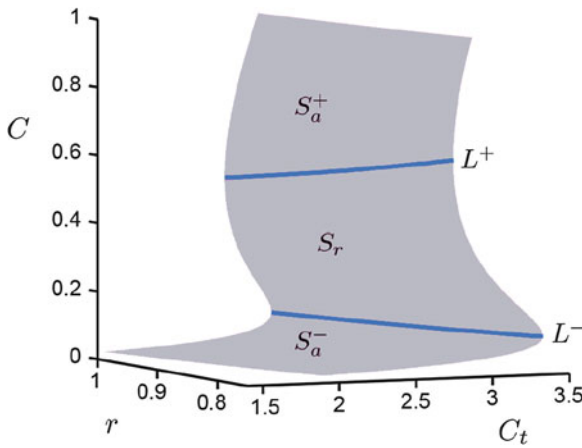


**Fig. 10** The critical manifold of the Class I Atri model, equations (2.32) with  $\alpha = 0$ ,  $\hat{\tau} = 0.48$ ,  $\hat{\nu} = 0.317$  and with fixed  $P = 0.95$ . The surface is divided into three branches (labelled  $S_a^\pm$  and  $S_r$ ) by the folds  $L^-$  and  $L^+$ . Figure modified from [61]

upper fold, make a fast jump to the lower branch of the critical manifold ( $S_a^-$ ), move slowly towards the lower fold, and then make a second fast jump back to  $S_a^+$ . For many parameter values, this singular orbit perturbs when  $\epsilon \neq 0$  to an RO or MMO, just as discussed in section 3.1.

Up to this point, the GSPT analysis of the Class I Atri model is fairly standard, but the story becomes more complicated when trying to explain the response of the model to pulsing in  $IP_3$ . It was shown in [61] that within the two-dimensional surface of fold points there is a one-dimensional curve of distinguished fold points, called *folded singularities*, that can strongly influence the pulse response of orbits. In certain parameter regimes, pulsed orbits of the full system pass near to the position in phase space at which folded singularities would lie in the singular system; if these folded singularities are of *folded saddle* or *folded node* subtype, a delay in the resumption of oscillations is seen, but if the pulsed orbit stays away from folded saddles or nodes no such delay is observed. Further detail about the analysis of the Class I model is contained in [61], with summary information about folded singularities being given in the review article [34] and the extension of the theory to the case of relevance here (i.e., a system with one fast and three slow variables) being presented in [150].

The next step to understanding the pulse response of the combined model was to look at the Class II model. GSPT methods were used in [61] to show that an unrelated mechanism is responsible for the delay in the pulse response of the Class II model. It was shown that pulsing the Class II model typically sends orbits into a region of phase space where the critical manifold is not folded, meaning that oscillations of the type seen in the Class II model without pulsing (i.e., ROs) are not possible. The pulsed orbit has to spend some time, corresponding to the observed phase lag, travelling back to the region of phase space where the critical manifold is folded before oscillations can resume.

This example is a nice illustration of the power of GSPT in explaining the dynamics of calcium models: the simplest approach, which assumed there is just one slow variable, was not able to properly explain the observations, and a rigorous approach using GSPT was needed. This example also provides an instance in which physiological considerations (i.e., the desire to explain the pulse responses) stimulated the development of new mathematics (e.g., the extension of GSPT to the case of three or more slow variables [150]).

## 4 Merging calcium dynamics and membrane electrical excitability

Many of the techniques used in the study of  $Ca^{2+}$  oscillations were developed in studies of the generation of oscillatory action potentials in neurons and other excitable cells. The membrane potential is by far the best known, and most widely studied, cellular oscillator, with most theoretical work based ultimately on the 1952

model of Hodgkin and Huxley [65]. It is far beyond the scope of the present work to discuss membrane potential models in detail; introductions to the theoretical study of membrane oscillators can be found in [73, 76].

However, no discussion of  $\text{Ca}^{2+}$  oscillations would be complete without at least a brief mention of how they interact with membrane potential oscillators. As a general rule, oscillations in the membrane potential (usually taking the form of oscillatory spiking) are caused by oscillatory opening and closing of ion channels (typically  $\text{Na}^+$ ,  $\text{K}^+$  or  $\text{Ca}^{2+}$  channels) in the cell membrane. Such oscillations in the membrane potential typically occur on a millisecond time scale, orders of magnitude faster than the  $\text{Ca}^{2+}$  oscillations discussed here.

However, many cells have ion channels whose conductances are controlled by  $[\text{Ca}^{2+}]$ . In this case, slow oscillations in  $[\text{Ca}^{2+}]$  can be used to modulate, over a longer time scale, the properties of the fast electrical oscillation. For example, slow oscillations in  $[\text{Ca}^{2+}]$  can move the membrane potential model in and out of the oscillatory regime (by, say, slow modulation of the  $\text{K}^+$  conductance), resulting in bursts of action potentials, a phenomenon known as electrical bursting, and seen in a wide variety of neurons and neuroendocrine cells. The paper by Bertram et al. in this volume presents a detailed discussion of one such type of model. Other examples can be found in [64, 68], while a basic introduction to the field can be found in [73].

Such systems, which couple a slower cytosolic  $\text{Ca}^{2+}$  oscillator to a faster membrane potential oscillator, have the potential for a wide range of complex and interesting dynamical behaviours. From a mathematical point of view, the complexity may arise, in part at least, from the multitude of time scales involved; models of membrane potential oscillators typically have at least two time scales, and calcium oscillator models also typically have at least two time scales, so combined models will typically have three or more time scales, depending on the relative speeds of the slower variable(s) in the membrane potential model and the faster variable(s) in the calcium model. A comprehensive theory of dynamics in systems with more than two time scales has yet to be developed, but early work indicates that very complex phenomena can occur in this context [79, 80]. From a physiological view point, models that couple a cytosolic  $\text{Ca}^{2+}$  oscillator to a faster membrane potential oscillator have particular importance in the study of neuroendocrine cells [9, 10, 11, 49, 82, 84, 87, 110, 144, 143, 156], and thus in the study of hormonal control, and are sure to be a major area of mathematical and experimental research in the future.

## 5 Calcium diffusion and waves

### 5.1 Basic equations

To turn a simple spatially homogeneous model into a model that allows for a spatially varying  $[\text{Ca}^{2+}]$  (as is, of course, the case in reality), the model equations must be adapted to include the diffusion of  $\text{Ca}^{2+}$ , and this requires, in practice, a host of additional assumptions.

Firstly, rather than modelling the ER and the cytoplasm as two distinct spaces, connected by  $\text{Ca}^{2+}$  fluxes, it is sufficient for most applications to combine these regions into a single homogenised domain, in which the ER and the cytoplasm co-exist at every point in space, and  $\text{Ca}^{2+}$  within each space has an effective diffusion coefficient that depends on the exact geometry assumed in the homogenisation [54]. Thus, we get the following equations for evolution of  $c$  and  $c_e$ :

$$\frac{\partial c}{\partial t} = \nabla \cdot (D_c^{\text{eff}} \nabla c) + \chi_c f(c, c_e), \quad (2.35)$$

$$\frac{\partial c_e}{\partial t} = \nabla \cdot (D_e^{\text{eff}} \nabla c_e) + \chi_e g(c, c_e), \quad (2.36)$$

where  $D_c^{\text{eff}}$  and  $D_e^{\text{eff}}$  are effective diffusion coefficients for the cytoplasmic space and the ER, respectively,  $\chi_c$  and  $\chi_e$  are the surface-to-volume ratios of these two co-mingled spaces, and  $f(c, c_e)$  and  $g(c, c_e)$  denote all the other  $\text{Ca}^{2+}$  fluxes and reactions.

It is usually assumed that the cellular cytoplasm is isotropic and homogeneous. It is not known, however, how  $\text{Ca}^{2+}$  diffuses in the ER, or the extent to which the tortuosity of the ER plays a role in determining the effective diffusion coefficient of ER  $\text{Ca}^{2+}$ . Thus, it is typical (and reasonable) to assume either that  $\text{Ca}^{2+}$  does not diffuse in the ER, or that it does so with a restricted diffusion coefficient,  $D_e^{\text{eff}} \ll D_c^{\text{eff}}$ . Henceforth we delete the superscript eff.

In this case, the simplified equations for  $\text{Ca}^{2+}$  diffusion are

$$\frac{\partial c}{\partial t} = D_c \nabla^2 c + f(c, c_e) + k_- b - k_+ c(b_t - b), \quad (2.37)$$

$$\frac{\partial c_e}{\partial t} = D_e \nabla^2 c_e + g(c, c_e), \quad (2.38)$$

$$\frac{\partial b}{\partial t} = D_b \nabla^2 b - k_- b + k_+ c(b_t - b), \quad (2.39)$$

where  $\chi_c$  and  $\chi_e$  have been absorbed into the other model parameters, and where cytoplasmic  $\text{Ca}^{2+}$  buffering has been explicitly included, for reasons that will become clear soon. ER  $\text{Ca}^{2+}$  buffering is not included explicitly, purely for simplicity. To do so makes no difference to the analysis, it merely makes the notation more complex.

As in the absence of diffusion, when buffering is fast the model can be condensed [122, 123, 147]. Assuming, as before, that

$$k_- b - k_+ c(b_t - b) = 0, \quad (2.40)$$

we get the “slow” equation

$$\frac{\partial}{\partial t}(c + b) = D_c \nabla^2 c + D_b \nabla^2 b + f(c, c_e), \quad (2.41)$$

which, after eliminating  $b$ , becomes

$$\frac{\partial c}{\partial t} = \frac{1}{1 + \theta(c)} \left( \nabla^2 \left( D_c c + D_b b_t \frac{c}{K + c} \right) + f(c, c_e) \right) \quad (2.42)$$

$$= \frac{D_c + D_b \theta(c)}{1 + \theta(c)} \nabla^2 c - \frac{2D_b \theta(c)}{(K + c)(1 + \theta(c))} |\nabla c|^2 + \frac{f(c, c_e)}{1 + \theta(c)}, \quad (2.43)$$

where, as before,

$$\theta(c) = \frac{b_t K}{(K + c)^2}. \quad (2.44)$$

Note that we assume that  $b_t$  does not vary in either space or time. A similar equation holds for  $c_e$ .

Nonlinear buffering changes the model structure significantly, although it can have surprisingly little qualitative effect on the resulting dynamics [52, 140]. In particular,  $\text{Ca}^{2+}$  obeys a nonlinear diffusion–advection equation, where the advection is the result of  $\text{Ca}^{2+}$  transport by a mobile buffer. The effective diffusion coefficient

$$D_{\text{eff}} = \frac{D_c + D_b \theta(c)}{1 + \theta(c)} \quad (2.45)$$

is a convex linear combination of the two diffusion coefficients  $D_c$  and  $D_b$ , so lies somewhere between the two. Since buffers are large molecules,  $D_{\text{eff}} < D_c$ . If the buffer is not mobile, i.e.,  $D_b = 0$ , then (2.43) reverts to a reaction–diffusion equation. Also, when  $\text{Ca}^{2+}$  gradients are small, the nonlinear advective term can be ignored.

If the buffer is not only fast, but also of low affinity, so that  $K \gg c$ , then  $\theta$  is constant, and  $D_{\text{eff}}$  is constant also.

It is commonly assumed that the buffer has fast kinetics, is immobile, and has a low affinity. With these assumptions we get the simplest possible model of  $\text{Ca}^{2+}$  buffers (short of not including them at all), in which

$$\frac{\partial c}{\partial t} = \frac{K}{K + b_t} (D_c \nabla^2 c + f(c)), \quad (2.46)$$

wherein both the diffusion coefficient and the fluxes are scaled by the constant factor  $K/(K + b_t)$ ; each flux in the model can then be interpreted as an *effective* flux, i.e., that fraction of the flux that contributes to a change in free  $\text{Ca}^{2+}$  concentration.

## 5.2 Fire-diffuse-fire models

One particularly simple way in which calcium excitability can be used to model waves is with the fire-diffuse-fire model [32, 75, 25, 28, 29], a direct analogue of the spike-diffuse-spike model of action potential propagation [26, 27]. In this

model, once  $[\text{Ca}^{2+}]$  reaches a threshold value,  $c^*$ , at a release site, that site fires, instantaneously releasing a fixed amount,  $\sigma$ , of  $\text{Ca}^{2+}$ . Thus, a  $\text{Ca}^{2+}$  wave is propagated by the sequential firing of release sites, each responding to the  $\text{Ca}^{2+}$  diffusing from neighbouring release sites. Hence the name fire–diffuse–fire.

In the fire–diffuse–fire model  $\text{Ca}^{2+}$  obeys the reaction–diffusion equation

$$\frac{\partial c}{\partial t} = D_c \frac{\partial^2 c}{\partial x^2} + \sigma \sum_n \delta(x - nL) \delta(t - t_n), \quad (2.47)$$

where  $L$  is the spacing between release sites. Although this equation looks linear, appearances are deceptive. Here,  $t_n$  is the time at which  $c$  first reaches the threshold value  $c^*$  at the  $n$ th release site, and thus depends in a complicated way on  $c$ .

The  $\text{Ca}^{2+}$  profile resulting from the firing of a single site, site  $i$ , say, is

$$c_i(x, t) = \sigma \frac{H(t - t_i)}{\sqrt{4\pi D_c(t - t_i)}} \exp\left(-\frac{(x - iL)^2}{4D_c(t - t_i)}\right), \quad (2.48)$$

where  $H$  is the Heaviside function. This is the fundamental solution of the diffusion equation with a delta function input at  $x = i$ ,  $t = t_i$ . If we superimpose the solutions from each site, we get

$$c(x, t) = \sum_i c_i(x, t) = \sigma \sum_i \frac{H(t - t_i)}{\sqrt{4\pi D_c(t - t_i)}} \exp\left(-\frac{(x - iL)^2}{4D_c(t - t_i)}\right). \quad (2.49)$$

Notice that because of the instantaneous release,  $c(x, t)$  is not a continuous function of time at any release site.

From this explicit expression it is possible to calculate an explicit expression for the wave speed. For full details the reader is referred to the abbreviated discussion in [73] or the more detailed presentations in the original articles referenced above.

This version of the fire–diffuse–fire model has no  $\text{Ca}^{2+}$  removal, and thus the concentration of  $\text{Ca}^{2+}$  is always increasing. This can be remedied by the inclusion of a  $\text{Ca}^{2+}$  removal term [25], modelling the removal by SERCA pumps. However, in order to preserve the analytical tractability of this approach, the removal term must be linear.

### 5.3 Another simple example

To illustrate some of the main features of wave propagation in  $\text{Ca}^{2+}$  models, we use a model similar to the combined model of Section 2.4, but somewhat simpler. Firstly, we include diffusion in one spatial dimension only. Even though  $\text{Ca}^{2+}$  waves propagate in three dimensions, a model in one spatial dimension is not necessarily a bad approximation. Since the wavelength of a typical  $\text{Ca}^{2+}$  wave is

large compared to the dimensions of a typical cell, much (but not all) intracellular wave propagation is essentially one-dimensional in nature. It is only when one considers wave propagation in much larger cells, such as a *Xenopus* oocyte, that the two and three dimensional properties of the waves become apparent, as the waves form spirals and target patterns [83].

We make a number of additional simplifications. Firstly, we assume that the  $\text{Ca}^{2+}$  ATPase pumps are linearly dependent on  $[\text{Ca}^{2+}]$ . Since we know this to be untrue, our simplified model will never be a good quantitative description of real  $\text{Ca}^{2+}$  waves. However, much of the underlying dynamical behaviour is preserved by this assumption. Secondly, we assume that the flux through the IPR is a bell-shaped function of  $[\text{Ca}^{2+}]$ , with no time delays. Hence, our simplified model here is neither a Class I nor a Class II model. In this case, the oscillations in  $[\text{Ca}^{2+}]$  are entirely dependent on  $\text{Ca}^{2+}$  influx from the outside. Although this is the case in only some cell types, the model still serves to illustrate the basic dynamical properties of  $\text{Ca}^{2+}$  models.

With these assumptions, our model equations are

$$\begin{aligned}\frac{\partial c}{\partial t} &= D_c \frac{\partial^2 c}{\partial x^2} + J_{\text{IPR}} - k_s c + \varepsilon(J_{\text{influx}} - k_p c), \\ \frac{\partial c_e}{\partial t} &= \gamma(-J_{\text{IPR}} + k_s c),\end{aligned}\tag{2.50}$$

where

$$J_{\text{influx}} = k_{\text{in}} p, \tag{2.51}$$

$$J_{\text{IPR}} = \left( \alpha + k_f p \left( \frac{c^2}{c^2 + \varphi_1^2} \right) \left( \frac{\varphi_2}{\varphi_2 + c} \right) \right) (c_e - c). \tag{2.52}$$

As before,  $p$  denotes  $[\text{IP}_3]$ , and is treated as the principal bifurcation parameter. The expression for  $J_{\text{influx}}$  is merely a slightly simplified version of equation (2.27). Because oscillations in this model depend on  $\text{Ca}^{2+}$  entry and exit from the cell, it is also possible to let  $J_{\text{influx}}$  be a parameter, and use it as the principal bifurcation parameter [142]. Typical values of the other model parameters are given in Table 2 in the Appendix.

## 5.4 CU systems

A convenient first step in investigating wave propagation in PDE models of calcium dynamics is to switch to a moving frame. For a model with one spatial variable,  $x$ , with solitary or periodic waves moving with a constant wave speed  $s$ , we can define a new variable,  $z = x + st$ , and rewrite the model in the moving frame. For instance, in terms of this new variable, the model given by equations (2.50) becomes:



$$\begin{aligned}
c' &= u, \\
u' &= \frac{1}{D_c} (su - J_{\text{IPR}} + k_s c - \varepsilon(J_{\text{influx}} - k_p c)), \\
c'_e &= \frac{\gamma}{s} (-J_{\text{IPR}} + k_s c),
\end{aligned} \tag{2.53}$$

where the prime denotes differentiation with respect to  $z$ .

We are interested in both pulse-type travelling waves and periodic travelling waves for the PDE model; in the moving frame ODEs, these correspond, respectively, to homoclinic orbits and periodic solutions. Typically, we will be interested in the existence of such solutions as both a bifurcation parameter of the PDE (e.g.,  $p$  for the model above) and  $s$ , the wave speed, vary. In the PDE formulation,  $s$  is a quantity selected by the dynamics, not a parameter of the equations, but in the travelling wave ODEs we treat  $s$  as a bifurcation parameter.

A first step is to look for homoclinic and Hopf bifurcations of the moving frame ODEs in the corresponding two-dimensional parameter space. For example, for the parameter values specified in Table 2, equations (2.53) have a unique equilibrium point, which is of saddle type with a one-dimensional unstable manifold and a two-dimensional stable manifold for  $p$  and  $s$  values outside the U-shaped curve labeled HB in Fig. 11. This equilibrium has a homoclinic bifurcation at  $(p, s)$  values on the C-shaped curve (labelled HC) in this figure.

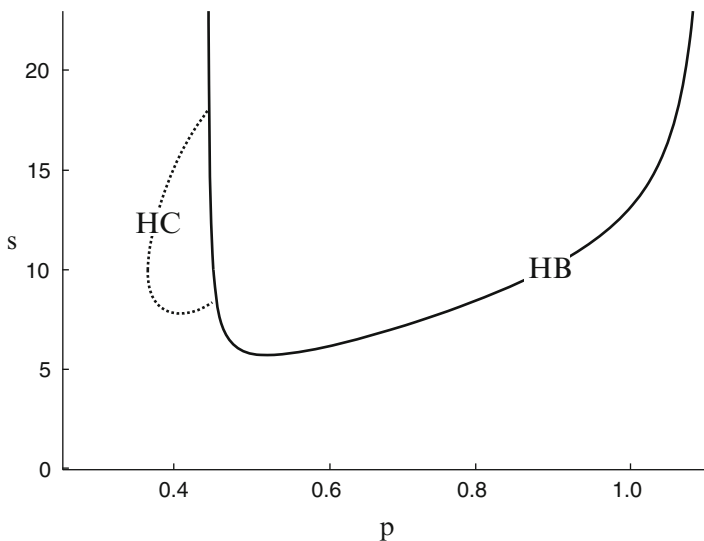


**Fig. 11** Partial bifurcation set for equations (2.53) for parameter values given in Table 2, showing a U-shaped curve of Hopf bifurcations (HB) and a C-shaped dotted curve of homoclinic bifurcations (HC)

The structure observed in Fig. 11, of a C-shaped homoclinic bifurcation curve and a U-shaped Hopf locus, turns out to be common to many models of calcium waves, as well as many other excitable systems such as the FitzHugh-Nagumo and Hodgkin-Huxley models [20]. It is argued in [20] and [142] that the CU-structure occurs as a consequence of the general shape of the nullclines in these models, which in turn follows from the underlying physiology. Furthermore, Maginu [90] showed that in the limit of  $s \rightarrow \infty$ , the travelling wave equations reduce to the model without diffusion (i.e., with  $D_c = 0$ ); since the diffusion-free version of a calcium model will typically have two Hopf bifurcations at finite values of the bifurcation parameter (as discussed in section 3), this result suggests that the Hopf locus really is U-shaped, i.e., the left and right arms of the Hopf locus will have vertical asymptotes at finite values of the bifurcation parameter.

For each fixed value of the main bifurcation parameter between the vertical asymptotes of the Hopf U there will typically be an interval of  $s$  values for which periodic solutions exist. It is natural to ask which of these periodic solutions will give stable periodic travelling waves in the PDE, i.e., to ask which wave speed will be selected by the PDE dynamics. There is no known general answer to this question; the answer is believed to depend on the precise boundary and initial conditions for the PDE. It is known [119] that very complicated, seemingly chaotic, travelling solutions can occur at values of the bifurcation parameter lying within the Hopf U.

Analysis of the moving frame ODEs can tell us about the existence of travelling waves in the associated PDE model, but does not give information about stability of these solutions in the PDEs. Instead, stability of travelling waves can be determined by direct computation (e.g., [109]) or by numerical computation on the PDEs (e.g., [119, 142]). In all the cases we have studied, it turns out that stable solitary travelling waves have wave speeds corresponding to the upper ‘branch’ (higher  $s$  values) of the C curve, although this branch may not be stable along its entire length. More complicated travelling pulses (e.g., with two pulses within the wave packet, corresponding to double-pulse homoclinic orbits in the travelling wave equations) may also occur [20] and can be stable [109].

Just as for ODE models, PDE models of calcium dynamics typically have processes occurring on two or more different time scales, and it is possible to exploit this time scale separation to explain model dynamics. Such ideas have been very successful in the analysis of the PDE version of the FitzHugh-Nagumo equations (e.g., [3, 72, 78]), but have been applied less to calcium models. One approach has been to look for the singular analogue of the CU structure, and to try to show that features of the bifurcation set of the full (non-singular) problem, including the CU structure, arise as perturbations of this singular structure. In [142], the existence and stability of travelling waves in a closed-cell (singular) version of a calcium model closely related to equations (2.53) was investigated theoretically, and the results compared with numerical results for the (non-singular) open-cell model. It was shown that the CU structure for the full system, found numerically, appears to converge in the singular limit to a collection of fronts, pulses and waves that

can be located analytically in the singular limit system and that form a singular CU structure. Work is underway to show rigorously how the singular CU structure perturbs to the nonsingular case.

Although the basic CU structure is common to many calcium models, other features of the bifurcation set vary from model to model. For instance, different models may exhibit a variety of different types of global bifurcations, including homoclinic and heteroclinic bifurcations of equilibria and periodic orbits [158], and give rise to a host of interesting issues from a bifurcation theory point of view, but these are not our focus in this article. One aspect of the dynamics of particular interest is how the C curve terminates near its apparent endpoints; this question has implications for the ways in which there can be a transition from stable travelling pulses to stable periodic travelling waves in the PDE and was discussed in [20, 119] for some specific models.

### 5.5 Calcium excitability and comparison to the FitzHugh-Nagumo equations

A crucially important feature of models of  $\text{Ca}^{2+}$  waves is excitability; a small amount of  $\text{Ca}^{2+}$  release induces the release of a larger amount of  $\text{Ca}^{2+}$  through positive feedback in the model. The most studied excitable system is the FitzHugh-Nagumo equations, and it has long been recognised that calcium waves propagate by an excitable mechanism similar in many ways to that in the FitzHugh-Nagumo model. Despite these similarities, however, there are important differences.

The FitzHugh-Nagumo equations can be written in the form

$$\begin{aligned}\frac{\partial u}{\partial t} &= D \frac{\partial^2 u}{\partial x^2} + u(u - \alpha)(1 - u) - w + I, \\ \frac{\partial w}{\partial t} &= \epsilon(u - \gamma w),\end{aligned}\tag{2.54}$$

where the variable  $u$  represents the plasma membrane electric potential,  $w$  represents the combined inactivation effects of the sodium and potassium channels, and  $I$  is the applied current. The parameter  $\epsilon$  satisfies  $0 \leq \epsilon \ll 1$ , and encodes the separation of time scales in the model,  $\alpha \in (0, \frac{1}{2})$ ,  $D$  is the diffusion constant and  $\gamma$  is a small positive constant [73]. Defining  $z = x + st$  in the usual way, where  $s$  is the wave speed, yields the model equations in the moving frame:

$$\begin{aligned}\frac{du}{dz} &= v, \\ \frac{dv}{dz} &= \frac{1}{D} (sv - u(u - \alpha)(1 - u) + w - I), \\ \frac{dw}{dz} &= \frac{\epsilon}{s} (u - \gamma w).\end{aligned}\tag{2.55}$$

In the absence of diffusion the dynamics of the FitzHugh-Nagumo equations and the dynamics of typical calcium models, such as equations (2.50), are qualitatively very similar. Any difference in dimension of the models (if the calcium model has three or more dependent variables) gives different possibilities for the detailed dynamics, but structural similarities in the models, specifically a clearly defined slow variable such as  $w$  for FitzHugh-Nagumo and  $c_i$  for calcium models, and the cubic shape of the nullcline for a fast variable ( $v$  for FitzHugh-Nagumo and  $c$  for calcium models), results in the diffusion-free models having similar bifurcation diagrams and time series. For instance, Fig. 12 shows bifurcation diagrams and typical time series for equations (2.50) with  $D_c = 0$  and for equations (2.54) with  $D = 0$ ; the similarities in the model dynamics are clear in these pictures.

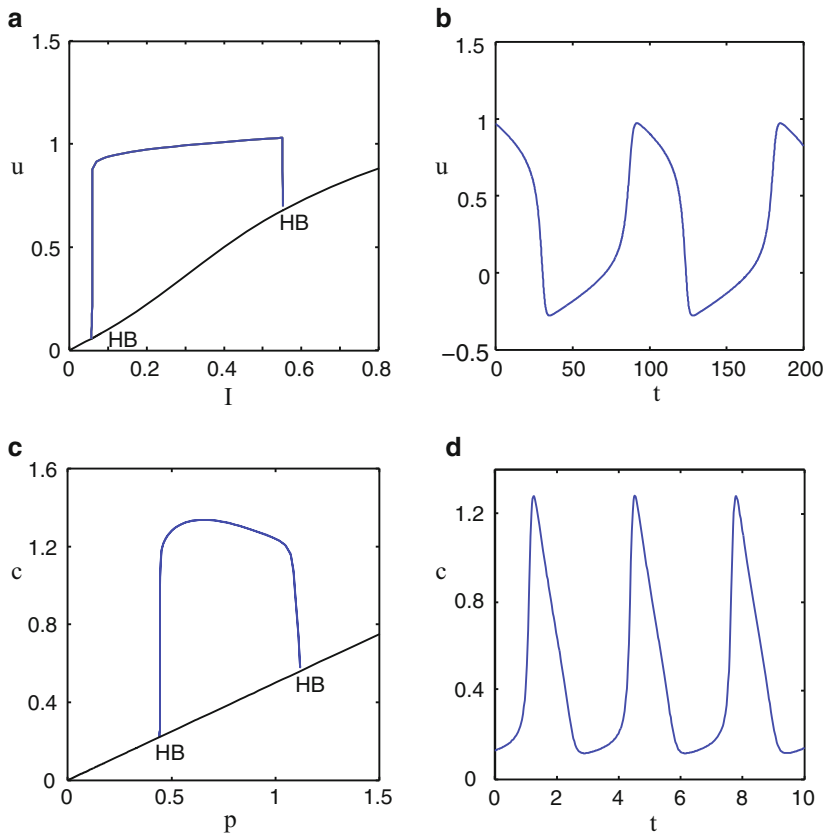


**Fig. 12** Bifurcation diagrams and time series for the FitzHugh-Nagumo model, equations (2.54), and a simple calcium model, equations (2.50) without diffusion. Panel A shows the bifurcation diagram for equations (2.54) with  $D = 0$ ,  $a = 0.1$ ,  $\gamma = 1.0$ ,  $\epsilon = 0.1$ . The black curve shows the position of the steady state solution and the blue curve indicates the maximum amplitudes of periodic orbits. Hopf bifurcations are labelled HB. Panel B shows the time series for the corresponding attracting periodic solution when  $I = 0.2$ . Panel C shows the bifurcation diagram for equations (2.50) with  $D_c = 0$  and other parameter values as in Table 1. Line styles and labels as for panel A. Panel D shows the time series for the corresponding attracting periodic solution when  $p = 0.7$ .

If diffusion is included, then there are still marked similarities between the dynamics of the FitzHugh-Nagumo equations and a typical calcium model. Most notably, the FitzHugh-Nagumo moving frame equations have a CU bifurcation structure in the  $(I, s)$  parameter plane very similar to that in calcium models [20, 142]. However, structural differences in the models mean that the underlying mechanisms can be quite different.

One important structural difference results from the way diffusion acts. In the FitzHugh-Nagumo model, diffusion appears in the evolution equation for the fast variable,  $u$ , only. This follows from a modelling assumption that the gating variable,  $w$ , is uniformly distributed along the spatial direction. The situation is, typically, different for calcium models, where diffusion affects both fast and slow variables since diffusion in the cytoplasm influences the evolution of both  $c$ , the cytoplasmic calcium concentration, and  $c_t$ , the total cellular concentration.

To see this in the case of equations (2.50) we go to the moving frame by setting  $z = x + st$  and  $u = dc/dz$ , then rewrite the model in standard fast-slow form by replacing  $c_e$  with  $c_t = s(c_e/\gamma + c) - D_c u$ . This definition of  $c_t$  is the PDE analogue of the total calcium variable introduced in section 2.4. With these changes, equations (2.53) become:

$$\begin{aligned} c' &= u, \\ u' &= \frac{1}{D_c} \left( su - \bar{J}_{\text{IPR}} \left( \frac{\gamma}{s} (c_t + D_c u - sc) - c \right) + k_s c - \varepsilon (J_{\text{influx}} - k_p c) \right), \\ c_t' &= \varepsilon (J_{\text{influx}} - k_p c), \end{aligned} \quad (2.56)$$

where the prime indicates differentiation with respect to  $z$  and

$$\bar{J}_{\text{IPR}} = \alpha + k_{fp} \left( \frac{c^2}{c^2 + \varphi_1^2} \right) \left( \frac{\varphi_2}{\varphi_2 + c} \right).$$

When  $\varepsilon$  is sufficiently small,  $c$  and  $u$  are fast variables and  $c_t$  is slow. One effect of the diffusion of calcium is, therefore, to introduce nonlinear coupling between the fast variables, i.e., a term of the form of  $ug(c)$  in the  $u'$  equation, for  $g(c)$  a nonlinear function of  $c$ . By comparison, in equations (2.55) there are no comparable terms in the differential equations for the fast variables.

A direct consequence of this difference is seen in the nature of the Hopf bifurcations. In the FitzHugh-Nagumo equations, the simple coupling between the fast variables means the Hopf bifurcations that occur on the vertical arms of the Hopf U are degenerate in the singular limit, in the sense that the bifurcation is neither supercritical or subcritical because the first Lyapunov coefficient is zero. For more generic coupling, as found in calcium models such as equations (2.50), this is not the case [142], and the Hopf bifurcations on the vertical arms will be either super- or sub-critical as the singular limit is approached. Note that in both types of model, the Hopf bifurcations are *singular Hopf* bifurcations in the singular limit (so that the imaginary parts of the eigenvalues at the Hopf bifurcations tend to

zero as  $\epsilon \rightarrow 0$ ; see [13]), but this singularity is distinct from the degeneracy arising from simple coupling in the FitzHugh-Nagumo equations. More work is needed to uncover exactly how this difference between the singular versions of the models influences the dynamics of the non-singular models.

A second important structural difference between the models occurs because the FitzHugh-Nagumo equations have a symmetry: equations (2.55) are equivariant with respect to the transformation

$$\begin{aligned} u &\rightarrow \frac{2}{3}(1 + \alpha) - u, & v &\rightarrow -v, & w &\rightarrow \frac{2}{3\gamma}(1 + \alpha) - w, \\ I &\rightarrow \frac{2}{3}(1 + \alpha) \left[ \frac{1}{\gamma} - \frac{(2 - \alpha)(1 - 2\alpha)}{9} \right] - I. \end{aligned}$$

As a consequence, some of the travelling pulses in the FitzHugh-Nagumo model arise as a perturbation of two symmetry-related singular travelling front solutions, corresponding in the moving frame to two symmetry-related heteroclinic orbits [142]. (Other travelling pulses arise as a perturbation of a singular travelling pulse, corresponding to a homoclinic orbit in the moving frame.) By contrast, calcium models typically do not have such a symmetry, and travelling wave solutions are unlikely to arise in this way. In a model closely related to equations (2.50) it appears that the corresponding travelling pulses also arise from the singular limit as a perturbation of travelling fronts [142], but the mechanism is more generic than in the FitzHugh-Nagumo model since it does not require the presence of symmetry. More work is necessary to establish whether this is the usual pattern in calcium models.

In summary, there are important structural differences between the FitzHugh-Nagumo equations and typical calcium models, which arise because of simplifying, non-generic assumptions made in constructing the FitzHugh-Nagumo equations. We conclude that models of calcium dynamics are excitable systems of a somewhat different type to the FitzHugh-Nagumo equations.

## 5.6 The effects on wave propagation of calcium buffers

Another way in which  $\text{Ca}^{2+}$  models differ from more widely studied models such as the FitzHugh-Nagumo equations is the presence of buffers. As discussed in Section 5.1,  $\text{Ca}^{2+}$  buffers effectively disappear from the model equations only under the rather restrictive assumptions of fast, linear, buffering. Since such assumptions are unlikely to be accurate in most cells, it is important to understand the dynamics of wave propagation in the presence of more general nonlinear or slow buffers. If the buffer is fast, but nonlinear, then we still have a single transport equation (equation (2.43)), but if the buffers are slow, then we are forced to deal with an additional equation (equation (2.39)).

The possible effects of buffers on waves are particularly interesting in the context of  $\text{Ca}^{2+}$  waves, as, experimentally,  $\text{Ca}^{2+}$  waves are observed by adding  $\text{Ca}^{2+}$  fluorescent dyes to cells. However, since these dyes are necessarily also  $\text{Ca}^{2+}$  buffers (as they must bind  $\text{Ca}^{2+}$  in order to emit light) questions have been raised about how much of the observed behaviour is an artefact of the experimental method. For example, is it possible for waves to exist only in the presence of the additional buffer represented by the dye, or do they exist even when they are not being measured?

There have been a number of studies, both numerical and analytic [69, 81, 99, 111, 122, 123, 121, 147], of the effects of  $\text{Ca}^{2+}$  buffers. By far the most analytical work on this question has been done by Je-Chiang Tsai [139, 140, 141, 142]. Almost all of this analytic work has been done on the FitzHugh-Nagumo model, the prototypical excitable system, or on the bistable equation, which is merely the FitzHugh-Nagumo model with no recovery variable. In the notation of this paper, the buffered bistable equation is just equation (2.37), with  $f(c, c_e) = c(1-c)(c-\alpha)$ , for some constant  $0 < \alpha < 1/2$ ; see [73] for an introductory discussion of wave propagation in the bistable and FitzHugh-Nagumo equations. As yet, it is not entirely clear how results from the buffered versions of the bistable or FitzHugh-Nagumo equations carry over to models of  $\text{Ca}^{2+}$  waves, but since these are the only excitable systems for which any significant amount of analytical work has been done, it is the best we can currently do. In addition, numerical solutions indicate that these analytical results carry over, in most part, to  $\text{Ca}^{2+}$  waves. Although this is not a proof, of course, it offers some reassurance.

Tsai has shown that, when the buffers are fast, there is a unique, stable, travelling wave solution to the buffered bistable equation, a result entirely analogous to the result for the unbuffered bistable equation. If the buffers are slow and immobile then, again, the same results holds; i.e., there exists a unique, stable, travelling wave solution. It is important to note that these travelling waves, although their existence, uniqueness and stability is guaranteed, may well have quite different forms or profiles from waves in the unbuffered bistable equation.

When the buffers are slow and mobile, the situation is more complicated. It is possible to eliminate waves by the addition of enough slow, mobile, buffer, but, when the waves exist, they are still unique and stable.

The buffered FitzHugh-Nagumo equation is considerably more complicated, having, as it does, an additional equation for the recovery variable, and presently there are analytical results only for the case of fast buffering. In this case there is a complex relationship between the binding constant of the buffer (i.e., the ratio  $k_-/k_+$ , which determines how strong the buffer is), the excitability of the system ( $\alpha$ ), and the time scale separation ( $\varepsilon$ ). If there is too much buffer present, waves will not exist. However, in some conditions, waves can be made to exist by the addition of a small amount (but not too much) of weakly binding buffer. Our current knowledge of the buffered FitzHugh-Nagumo equation is summarised in [141], although many gaps remain.

6 Conclusion

This review has focused on only a very restricted range of models of  $\text{Ca}^{2+}$  dynamics, but even this small range suffices to show how these models raise a host of important mathematical questions. Not only are these questions proving to be vital for the interpretation of some experimental data, they also have applicability well outside the immediate area of  $\text{Ca}^{2+}$  dynamics, particularly in the study of membrane potential models, or models of chemical reactions with multiple time scales.

**Acknowledgements** This work was supported by the Marsden Fund of the Royal Society of New Zealand and by the National Institutes of Health of the USA (NIDCR R01DE019245).

Appendix

**Table 1** Values of parameters for the combined model, equations (2.20)–(2.23)

Parameter	Value	Parameter	Value	Parameter	Value
$b$	0.111	$k_2$	$0.7\ \mu\text{M}$	$k_{\text{flux}}$	$6\ \text{s}^{-1}$
$\delta$	0.01	$k_4$	$1.1\ \mu\text{M}$	$V_p$	$24.0\ \mu\text{M s}^{-1}$
$\gamma$	5.405	$k_p$	$0.4\ \mu\text{M}$	$V_e$	$20.0\ \mu\text{M s}^{-1}$
$\mu_0$	0.567	$k_e$	$0.06\ \mu\text{M}$	$\alpha_1$	$1.0\ \mu\text{M s}^{-1}$
$\mu_1$	0.433	$k_1$	$1.1\ \mu\text{M}$	$\alpha_2$	$0.2\ \text{s}^{-1}$
$V_1$	0.889	$k_\mu$	$4.0\ \mu\text{M}$	$\beta$	$0.08\ \text{s}^{-1}$

**Table 2** Values of parameters for the model defined by equations (2.50)

$\alpha$	$k_s$	$k_f$	$k_p$	$\varphi_1$	$\varphi_2$	$\varepsilon$	$\gamma$	$k_{\text{in}}$	$D_c$
$0.05\ \text{s}^{-1}$	$20\ \text{s}^{-1}$	$20\ \text{s}^{-1}$	$20\ \text{s}^{-1}$	$2\ \mu\text{M}$	$1\ \mu\text{M}$	0.1	5	$10\ \text{s}^{-1}$	$20\ \mu\text{m}^2\text{s}^{-1}$

References

[1] Ambudkar IS (2012) Polarization of calcium signaling and fluid secretion in salivary gland cells. *Curr Med Chem* 19(34):5774–81

[2] Atri A, Amundson J, Clapham D, Sneyd J (1993) A single-pool model for intracellular calcium oscillations and waves in the *Xenopus laevis* oocyte. *Biophys J* 65(4):1727–39, DOI [10.1016/S0006-3495\(93\)81191-3](https://doi.org/10.1016/S0006-3495(93)81191-3)

[3] Bell D, Deng B (2002) Singular perturbation of N-front travelling waves in the FitzHugh–Nagumo equations. *Nonlinear analysis: Real world applications* 3(4):515–541

[4] Berridge MJ (2009) Inositol trisphosphate and calcium signalling mechanisms. *Biochim Biophys Acta* 1793(6):933–40



- [5] Berridge MJ (2012) Calcium signalling remodelling and disease. *Biochem Soc Trans* 40(2):297–309
- [6] Berridge MJ, Lipp P, Bootman MD (2000) The versatility and universality of calcium signalling. *Nat Rev Mol Cell Biol* 1(1):11–21
- [7] Bers D (2000) Calcium fluxes involved in control of cardiac myocyte contraction. *Circ Res* 87(4):275–281
- [8] Bers DM (2001) Excitation-contraction coupling and cardiac contractile force. Second edition. Kluwer, New York
- [9] Bertram R (2005) A mathematical model for the mating-induced prolactin rhythm of female rats. *AJP: Endocrinology and Metabolism* 290(3):E573–E582
- [10] Bertram R, Previte J, Sherman A, Kinard TA, Satin LS (2000) The phantom burster model for pancreatic  $\beta$ -cells. *Biophys J* 79(6):2880–2892
- [11] Bertram R, Sherman A, Satin LS (2010) Electrical bursting, calcium oscillations, and synchronization of pancreatic islets. *Adv Exp Med Biol* 654:261–79
- [12] Bootman M, Niggli E, Berridge M, Lipp P (1997) Imaging the hierarchical  $\text{Ca}^{2+}$  signalling system in HeLa cells. *J Physiol* 499(2):307–14
- [13] Braaksma B (1998) Singular Hopf bifurcation in systems with fast and slow variables. *Journal of Nonlinear Science* 8:457–490
- [14] Brini M, Carafoli E (2009) Calcium pumps in health and disease. *Physiol Rev* 89(4):1341–1378
- [15] Callamaras N, Marchant JS, Sun XP, Parker I (1998) Activation and co-ordination of  $\text{InsP}_3$ -mediated elementary  $\text{Ca}^{2+}$  events during global  $\text{Ca}^{2+}$  signals in *Xenopus* oocytes. *J Physiol* 509(1):81–91
- [16] Cannell MB, Kong CHT (2012) Local control in cardiac E–C coupling. *Journal of Molecular and Cellular Cardiology* 52(2):298–303
- [17] Cannell MB, Soeller C (1999) Mechanisms underlying calcium sparks in cardiac muscle. *J Gen Physiol* 113(3):373–6
- [18] Cao P, Donovan G, Falcke M, Sneyd J (2013) A stochastic model of calcium puffs based on single-channel data. *Biophys J* 105(5):1133–42, DOI [10.1016/j.bpj.2013.07.034](https://doi.org/10.1016/j.bpj.2013.07.034)
- [19] Catterall WA (2011) Voltage-gated calcium channels. *Cold Spring Harb Perspect Biol* 3(8):a003947, DOI [10.1101/cshperspect.a003947](https://doi.org/10.1101/cshperspect.a003947)
- [20] Champneys A, Kirk V, Knobloch E, Oldeman B, Sneyd J (2007) When Shil'nikov meets Hopf in excitable systems. *SIAM J Appl Dyn Syst* 6:663–693
- [21] Cheer A, Nuccitelli R, Oster G, Vincent JP (1987) Cortical waves in vertebrate eggs I: the activation waves. *J Theor Biol* 124:377–404
- [22] Cheng H, Lederer WJ, Cannell MB (1993) Calcium sparks: elementary events underlying excitation-contraction coupling in heart muscle. *Science* 262(5134):740–4
- [23] Colegrove S, Albrecht M, Friel D (2000a) Quantitative analysis of mitochondrial  $\text{Ca}^{2+}$  uptake and release pathways in sympathetic neurons. reconstruction of the recovery after depolarization-evoked  $[\text{Ca}^{2+}]_i$  elevations. *J Gen Physiol* 115:371–88
- [24] Colegrove SL, Albrecht MA, Friel D (2000b) Dissection of mitochondrial  $\text{Ca}^{2+}$  uptake and release fluxes in situ after depolarization-evoked  $[\text{Ca}^{2+}]_i$  elevations in sympathetic neurons. *J Gen Physiol* 115(3):351–370
- [25] Coombes S (2001a) The effect of ion pumps on the speed of travelling waves in the fire-diffuse-fire model of  $\text{Ca}^{2+}$  release. *Bull Math Biol* 63(1):1–20
- [26] Coombes S (2001b) From periodic travelling waves to travelling fronts in the spike-diffuse-spike model of dendritic waves. *Math Biosci* 170(2):155–72
- [27] Coombes S, Bressloff PC (2003) Saltatory waves in the spike-diffuse-spike model of active dendritic spines. *Phys Rev Lett* 91(2):028,102
- [28] Coombes S, Timofeeva Y (2003) Sparks and waves in a stochastic fire-diffuse-fire model of  $\text{Ca}^{2+}$  release. *Phys Rev E Stat Nonlin Soft Matter Phys* 68(2 Pt 1):021,915
- [29] Coombes S, Hinch R, Timofeeva Y (2004) Receptors, sparks and waves in a fire-diffuse-fire framework for calcium release. *Prog Biophys Mol Biol* 85(2–3):197–216

- [30] Cuthbertson KSR, Chay T (1991) Modelling receptor-controlled intracellular calcium oscillators. *Cell Calcium* 12:97–109
- [31] Dash RK, Qi F, Beard DA (2009) A biophysically based mathematical model for the kinetics of mitochondrial calcium uniporter. *Biophys J* 96(4):1318–1332
- [32] Dawson SP, Keizer J, Pearson JE (1999) Fire-diffuse-fire model of dynamics of intracellular calcium waves. *Proc Natl Acad Sci U S A* 96(11):6060–6063
- [33] De Young G, Keizer J (1992) A single pool IP<sub>3</sub>-receptor based model for agonist stimulated Ca<sup>2+</sup> oscillations. *Proc Natl Acad Sci U S A* 89:9895–9899
- [34] Desroches M, Guckenheimer J, Krauskopf B, Kuehn C (2012) Mixed-mode oscillations with multiple time scales. *SIAM Review* 54(2):211–288
- [35] Domijan M, Murray R, Sneyd J (2006) Dynamical probing of the mechanisms underlying calcium oscillations. *J Nonlin Sci* 16(5):483–506
- [36] Dufour JF, Arias I, Turner T (1997) Inositol 1,4,5-trisphosphate and calcium regulate the calcium channel function of the hepatic inositol 1,4,5-trisphosphate receptor. *J Biol Chem* 272:2675–2681
- [37] Dupont G, Erneux C (1997) Simulations of the effects of inositol 1,4,5-trisphosphate 3-kinase and 5-phosphatase activities on Ca<sup>2+</sup> oscillations. *Cell Calcium* 22(5):321–31
- [38] Dupont G, Combettes L, Leybaert L (2007) Calcium dynamics: spatio-temporal organization from the subcellular to the organ level. *Int Rev Cytol* 261:193–245
- [39] Dupont G, Combettes L, Bird GS, Putney JW (2011) Calcium oscillations. *Cold Spring Harb Perspect Biol* 3(3)
- [40] Endo M (2009) Calcium-induced calcium release in skeletal muscle. *Physiol Rev* 89(4):1153–76
- [41] Endo M, Tanaka M, Ogawa Y (1970) Calcium-induced release of calcium from the sarcoplasmic reticulum of skinned skeletal muscle fibres. *Nature* 228:34–36
- [42] Falcke M (2003a) Buffers and oscillations in intracellular Ca<sup>2+</sup> dynamics. *Biophys J* 84(1):28–41
- [43] Falcke M (2003b) Deterministic and stochastic models of intracellular Ca<sup>2+</sup> waves. *New Journal of Physics* 5:96
- [44] Falcke M (2004) Reading the patterns in living cells – the physics of Ca<sup>2+</sup> signaling. *Advances in Physics* 53(3):255–440
- [45] Falcke M, Hudson JL, Camacho P, Lechleiter JD (1999) Impact of mitochondrial Ca<sup>2+</sup> cycling on pattern formation and stability. *Biophys J* 77(1):37–44
- [46] Fill M, Copello JA (2002) Ryanodine receptor calcium release channels. *Physiol Rev* 82(4):893–922
- [47] Fill M, Zahradníková A, Villalba-Galea CA, Zahradník I, Escobar AL, Györke S (2000) Ryanodine receptor adaptation. *J Gen Physiol* 116(6):873–82
- [48] Finch E, Goldin S (1994) Calcium and inositol 1,4,5-trisphosphate-induced Ca<sup>2+</sup> release. *Science* 265:813–815
- [49] Fletcher PA, Li YX (2009) An integrated model of electrical spiking, bursting, and calcium oscillations in GnRH neurons. *Biophys J* 96(11):4514–24
- [50] Foscett JK, White C, Cheung KH, Mak DOD (2007) Inositol trisphosphate receptor Ca<sup>2+</sup> release channels. *Physiol Rev* 87(2):593–658
- [51] Friel DD (1995) [Ca<sup>2+</sup>]<sub>i</sub> oscillations in sympathetic neurons: an experimental test of a theoretical model. *Biophys J* 68(5):1752–1766
- [52] Gin E, Kirk V, Sneyd J (2006) A bifurcation analysis of calcium buffering. *J Theor Biol* 242(1):1–15
- [53] Gin E, Crampin EJ, Brown DA, Shuttleworth TJ, Yule DI, Sneyd J (2007) A mathematical model of fluid secretion from a parotid acinar cell. *J Theor Biol* 248(1):64–80
- [54] Goel P, Sneyd J, Friedman A (2006) Homogenization of the cell cytoplasm: the calcium bidomain equations. *SIAM J Multiscale Modeling and Simulation* 5:1045–1062
- [55] Goldbeter A, Dupont G, Berridge M (1990) Minimal model for signal-induced Ca<sup>2+</sup> oscillations and for their frequency encoding through protein phosphorylation. *Proc Natl Acad Sci USA* 87:1461–1465

- [56] Greenstein JL, Winslow RL (2011) Integrative systems models of cardiac excitation-contraction coupling. *Circ Res* 108(1):70–84
- [57] Greenstein JL, Hinch R, Winslow RL (2006) Mechanisms of excitation-contraction coupling in an integrative model of the cardiac ventricular myocyte. *Biophys J* 90(1):77–91
- [58] Groff JR, Smith GD (2008) Calcium-dependent inactivation and the dynamics of calcium puffs and sparks. *J Theor Biol* 253(3):483–99
- [59] Grubelnik V, Larsen AZ, Kummer U, Olsen LF, Marhl M (2001) Mitochondria regulate the amplitude of simple and complex calcium oscillations. *Biophys Chem* 94(1–2):59–74
- [60] Haak LL, Song LS, Molinski TF, Pessah IN, Cheng H, Russell JT (2001) Sparks and puffs in oligodendrocyte progenitors: cross talk between ryanodine receptors and inositol triphosphate receptors. *Journal of Neuroscience* 21(11):3860–3870
- [61] Harvey E, Kirk V, Osinga HM, Sneyd J, Wechselberger M (2010) Understanding anomalous delays in a model of intracellular calcium dynamics. *Chaos* 20(4):045,104
- [62] Harvey E, Kirk V, Wechselberger M, Sneyd J (2011) Multiple timescales, mixed mode oscillations and canards in models of intracellular calcium dynamics. *J Nonlin Sci* 21(5):639–683
- [63] Higgins ER, Cannell MB, Sneyd J (2006) A buffering SERCA pump in models of calcium dynamics. *Biophys J* 91(1):151–63
- [64] Hindmarsh JL, Rose RM (1984) A model of neuronal bursting using three coupled first order differential equations. *Proc R Soc Lond B* 221:87–102
- [65] Hodgkin AL, Huxley AF (1952) A quantitative description of membrane current and its application to conduction and excitation in nerve. *J Physiol* 117(4):500–44
- [66] Ilyin V, Parker I (1994) Role of cytosolic  $\text{Ca}^{2+}$  in inhibition of  $\text{InsP}_3$ -evoked  $\text{Ca}^{2+}$  release in *Xenopus* oocytes. *J Physiol* 477 ( Pt 3):503–9
- [67] Ionescu L, White C, Cheung KH, Shuai J, Parker I, Pearson JE, Foscett JK, Mak DO (2007) Mode switching is the major mechanism of ligand regulation of  $\text{InsP}_3$  receptor calcium release channels. *J Gen Physiol* 130(6):631–45
- [68] Izhikevich E (2000) Neural excitability, spiking and bursting. *Int J Bif Chaos* 10(6):1171–1266
- [69] Jafri M (1995) A theoretical study of cytosolic calcium waves in *Xenopus* oocytes. *J Theor Biol* 172:209–216
- [70] Janssen LJ, Kwan CY (2007) ROCs and SOC: What’s in a name? *Cell Calcium* 41(3):245–247
- [71] Jasoni CL, Romano N, Constantin S, Lee K, Herbison AE (2010) Calcium dynamics in gonadotropin-releasing hormone neurons. *Front Neuroendocrinol* 31(3):259–69
- [72] Jones C (1984) Stability of the traveling wave solutions of the FitzHugh-Nagumo system. *Trans Amer Math Soc* 286:431–469
- [73] Keener J, Sneyd J (2008) *Mathematical Physiology*, 2nd edn. Springer-Verlag, New York
- [74] Keizer J, Li YX, Stojilković S, Rinzel J (1995)  $\text{InsP}_3$ -induced  $\text{Ca}^{2+}$  excitability of the endoplasmic reticulum. *Mol Biol Cell* 6(8):945–51
- [75] Keizer J, Smith GD, Ponce-Dawson S, Pearson JE (1998) Saltatory propagation of  $\text{Ca}^{2+}$  waves by  $\text{Ca}^{2+}$  sparks. *Biophys J* 75(2):595–600
- [76] Koch C, Segev I (eds) (1998) *Methods in Neuronal Modeling; from Ions to Networks*. MIT Press, Cambridge, MA
- [77] Koivumäki JT, Takalo J, Korhonen T, Tavi P, Weckström M (2009) Modelling sarcoplasmic reticulum calcium ATPase and its regulation in cardiac myocytes. *Philosophical Transactions of the Royal Society A: Mathematical, Physical and Engineering Sciences* 367(1896):2181–2202
- [78] Krupa M, Sandstede B, Szmolyan P (1997) Fast and slow waves in the FitzHugh-Nagumo equation. *J Diff Eq* 133(1):49–97
- [79] Krupa M, Popovic N, Kopell N (2008) Mixed-mode oscillations in three time-scale systems: A prototypical example. *SIAM J Appl Dyn Syst* 7(2):361–420
- [80] Krupa M, Vidal A, Desroches M, Clément F (2012) Mixed-mode oscillations in a multiple time scale phantom bursting system. *SIAM J Appl Dyn Syst* 11(4):1458–1498

- [81] Kupferman R, Mitra P, Hohenberg P, Wang S (1997) Analytical calculation of intracellular calcium wave characteristics. *Biophys J* 72(6):2430–44
- [82] LeBeau AP, Robson AB, McKinnon AE, Donald RA, Sneyd J (1997) Generation of action potentials in a mathematical model of corticotrophs. *Biophys J* 73(3):1263–75
- [83] Lechleiter J, Girard S, Peralta E, Clapham D (1991) Spiral calcium wave propagation and annihilation in *xenopus laevis* oocytes. *Science* 252:123–126
- [84] Lee K, Duan W, Sneyd J, Herbison AE (2010) Two slow calcium-activated afterhyperpolarization currents control burst firing dynamics in gonadotropin-releasing hormone neurons. *J Neurosci* 30(18):6214–24
- [85] Leybaert L, Sanderson MJ (2012) Intercellular  $\text{Ca}^{2+}$  waves: mechanisms and function. *Physiol Rev* 92(3):1359–92
- [86] Li YX, Rinzel J (1994) Equations for  $\text{InsP}_3$  receptor-mediated  $\text{Ca}^{2+}$  oscillations derived from a detailed kinetic model: a Hodgkin-Huxley-like formalism. *J Theor Biol* 166:461–473
- [87] Li YX, Rinzel J, Keizer J, Stojilković S (1994) Calcium oscillations in pituitary gonadotrophs: comparison of experiment and theory. *Proc Natl Acad Sci USA* 91:58–62
- [88] Li YX, Rinzel J, Vergara L, Stojilković SS (1995) Spontaneous electrical and calcium oscillations in unstimulated pituitary gonadotrophs. *Biophys J* 69(3):785–95
- [89] MacLennan DH, Rice WJ, Green NM (1997) The mechanism of  $\text{Ca}^{2+}$  transport by sarco(endo)plasmic reticulum  $\text{Ca}^{2+}$ -ATPases. *J Biol Chem* 272(46):28,815–8
- [90] Maginu K (1985) Geometrical characteristics associated with stability and bifurcations of periodic travelling waves in reaction-diffusion equations. *SIAM J Appl Math* 45:750–774
- [91] Magnus G, Keizer J (1997) Minimal model of beta-cell mitochondrial  $\text{Ca}^{2+}$  handling. *Am J Physiol* 273(2 Pt 1):C717–C733
- [92] Magnus G, Keizer J (1998) Model of beta-cell mitochondrial calcium handling and electrical activity. i. cytoplasmic variables. *Am J Physiol* 274(4 Pt 1):C1158–C1173
- [93] Mak DOD, Pearson JE, Loong KPC, Datta S, Fernández-Mongil M, Foskett JK (2007) Rapid ligand-regulated gating kinetics of single inositol 1,4,5-trisphosphate receptor  $\text{Ca}^{2+}$  release channels. *EMBO Rep* 8(11):1044–51
- [94] Marchant JS, Parker I (2001) Role of elementary  $\text{Ca}^{2+}$  puffs in generating repetitive  $\text{Ca}^{2+}$  oscillations. *EMBO J* 20(1–2):65–76
- [95] Marhl M, Habrichter T, Brumen M, Heinrich R (2000) Complex calcium oscillations and the role of mitochondria and cytosolic proteins. *Biosystems* 57:75–86
- [96] Meinrenken CJ, Borst JG, Sakmann B (2003) Local routes revisited: the space and time dependence of the  $\text{Ca}^{2+}$  signal for phasic transmitter release at the rat calyx of Held. *J Physiol* 547(Pt 3):665–89
- [97] Møller JV, Olesen C, Winther AML, Nissen P (2010) The sarcoplasmic  $\text{Ca}^{2+}$ -ATPase: design of a perfect chemi-osmotic pump. *Quart Rev Biophys* 43(04):501–566
- [98] Neher E, Augustine GJ (1992) Calcium gradients and buffers in bovine chromaffin cells. *J Physiol* 450:273–301
- [99] Neher E, Sakaba T (2008) Multiple roles of calcium ions in the regulation of neurotransmitter release. *Neuron* 59(6):861–72, DOI [10.1016/j.neuron.2008.08.019](https://doi.org/10.1016/j.neuron.2008.08.019)
- [100] Neher EE (1995) The use of fura-2 for estimating Ca buffers and Ca fluxes. *Neuropharmacology* 34(11):1423–1442
- [101] Palk L, Sneyd J, Shuttleworth TJ, Yule DI, Crampin EJ (2010) A dynamic model of saliva secretion. *J Theor Biol* 266(4):625–40
- [102] Palk L, Sneyd J, Patterson K, Shuttleworth TJ, Yule DI, Maclaren O, Crampin EJ (2012) Modelling the effects of calcium waves and oscillations on saliva secretion. *J Theor Biol* 305:45–53
- [103] Parekh AB, Putney JW (2005) Store-operated calcium channels. *Physiol Rev* 85(2):757–810
- [104] Perez JF, Sanderson MJ (2005) The frequency of calcium oscillations induced by 5-HT, ACH, and KCl determine the contraction of smooth muscle cells of intrapulmonary bronchioles. *J Gen Physiol* 125(6):535–53
- [105] Politi A, Gaspers LD, Thomas AP, Höfer T (2006) Models of  $\text{IP}_3$  and  $\text{Ca}^{2+}$  oscillations: frequency encoding and identification of underlying feedbacks. *Biophys J* 90(9):3120–33

- [106] Pradhan RK, Beard DA, Dash RK (2010) A biophysically based mathematical model for the kinetics of mitochondrial  $\text{Na}^+$ - $\text{Ca}^{2+}$  antiporter. *Biophys J* 98(2):218–230
- [107] Ressmeyer AR, Bai Y, Delmotte P, Uy KF, Thistlethwaite P, Fraire A, Sato O, Ikebe M, Sanderson MJ (2010) Human airway contraction and formoterol-induced relaxation is determined by  $\text{Ca}^{2+}$  oscillations and  $\text{Ca}^{2+}$  sensitivity. *Am J Respir Cell Mol Biol* 43(2):179–91
- [108] Rinzel J (1985) Bursting oscillations in an excitable membrane model. In: Sleeman B, Jarvis R (eds) *Ordinary and partial differential equations*, Springer-Verlag, New York
- [109] Romeo MM, Jones CKRT (2003) The stability of traveling calcium pulses in a pancreatic acinar cell. *Physica D* 177(1):242–258
- [110] Roper P, Callaway J, Armstrong W (2004) Burst initiation and termination in phasic vasopressin cells of the rat supraoptic nucleus: a combined mathematical, electrical, and calcium fluorescence study. *J Neurosci* 24(20):4818–31, DOI [10.1523/JNEUROSCI.4203-03.2004](https://doi.org/10.1523/JNEUROSCI.4203-03.2004)
- [111] Sala F, Hernández-Cruz A (1990) Calcium diffusion modeling in a spherical neuron: relevance of buffering properties. *Biophys J* 57:313–324
- [112] Salido GM, Sage SO, Rosado JA (2009) TRPC channels and store-operated  $\text{Ca}^{2+}$  entry. *BBA - Molecular Cell Research* 1793(2):223–230
- [113] Sanderson MJ, Bai Y, Perez-Zoghbi J (2010)  $\text{Ca}^{2+}$  oscillations regulate contraction of intrapulmonary smooth muscle cells. *Adv Exp Med Biol* 661:77–96
- [114] Schuster S, Marhl M, Höfer T (2002) Modelling of simple and complex calcium oscillations. From single-cell responses to intercellular signalling. *Eur J Biochem* 269(5):1333–55
- [115] Shannon TR, Wang F, Puglisi J, Weber C, Bers DM (2004) A mathematical treatment of integrated Ca dynamics within the ventricular myocyte. *Biophys J* 87(5):3351–71
- [116] Shuai J, Pearson JE, Foscett JK, Mak DO, Parker I (2007) A kinetic model of single and clustered  $\text{IP}_3$  receptors in the absence of  $\text{Ca}^{2+}$  feedback. *Biophys J* 93(4):1151–62
- [117] Shuttleworth TJ (2012) STIM and Orai proteins and the non-capacitative ARC channels. *Front Biosci* 17:847–60
- [118] Siekmann I, Wagner LE, Yule D, Crampin EJ, Sneyd J (2012) A kinetic model for type I and II  $\text{IP}_3\text{R}$  accounting for mode changes. *Biophys J* 103(4):658–68
- [119] Simpson D, Kirk V, Sneyd J (2005) Complex oscillations and waves of calcium in pancreatic acinar cells. *Physica D: Nonlinear Phenomena* 200(3–4):303–324
- [120] Skupin A, Falcke M (2009) From puffs to global  $\text{Ca}^{2+}$  signals: how molecular properties shape global signals. *Chaos* 19(3):037,111
- [121] Smith G, Dai L, Miura R, Sherman A (2001) Asymptotic analysis of buffered calcium diffusion near a point source. *SIAM J on Appl Math* 61:1816–1838
- [122] Smith GD (1996) Analytical steady-state solution to the rapid buffering approximation near an open  $\text{Ca}^{2+}$  channel. *Biophys J* 71(6):3064–72
- [123] Smith GD, Wagner J, Keizer J (1996) Validity of the rapid buffering approximation near a point source of calcium ions. *Biophys J* 70(6):2527–39
- [124] Smyth JT, Hwang SY, Tomita T, DeHaven WI, Mercer JC, Putney JW (2010) Activation and regulation of store-operated calcium entry. *J Cell Mol Med* 14(10):2337–2349
- [125] Sneyd J, Dufour JF (2002) A dynamic model of the type-2 inositol trisphosphate receptor. *Proc Natl Acad Sci USA* 99(4):2398–403
- [126] Sneyd J, Falcke M (2005) Models of the inositol trisphosphate receptor. *Prog Biophys Mol Biol* 89(3):207–45
- [127] Sneyd J, Sherratt J (1997) On the propagation of calcium waves in an inhomogeneous medium. *SIAM J Appl Math* 57:73–94
- [128] Sneyd J, Dale P, Duffy A (1998) Traveling waves in buffered systems: applications to calcium waves. *SIAM J Appl Math* 58:1178–1192
- [129] Sneyd J, Tsaneva-Atanasova K, Yule DI, Thompson JL, Shuttleworth TJ (2004) Control of calcium oscillations by membrane fluxes. *Proc Natl Acad Sci USA* 101(5):1392–6, DOI [10.1073/pnas.0303472101](https://doi.org/10.1073/pnas.0303472101)

- [130] Sneyd J, Tsaneva-Atanasova K, Reznikov V, Bai Y, Sanderson MJ, Yule DI (2006) A method for determining the dependence of calcium oscillations on inositol trisphosphate oscillations. *Proc Natl Acad Sci USA* 103(6):1675–80, DOI [10.1073/pnas.0506135103](https://doi.org/10.1073/pnas.0506135103)
- [131] Soboloff J, Rothberg BS, Madesh M, Gill DL (2012) STIM proteins: dynamic calcium signal transducers. *Nat Rev Mol Cell Biol* 13(9):549–565
- [132] Soeller C, Cannell MB (2004) Analysing cardiac excitation-contraction coupling with mathematical models of local control. *Prog Biophys Mol Biol* 85(2–3):141–62
- [133] Straub SV, Giovannucci DR, Yule DI (2000) Calcium wave propagation in pancreatic acinar cells: functional interaction of inositol 1,4,5-trisphosphate receptors, ryanodine receptors, and mitochondria. *J Gen Physiol* 116(4):547–560
- [134] Tanimura A, Morita T, Nezu A, Tojyo Y (2009) Monitoring of IP<sub>3</sub> dynamics during Ca<sup>2+</sup> oscillations in HSY human parotid cell line with FRET-based IP<sub>3</sub> biosensors. *J Med Invest* 56 Suppl:357–61
- [135] Thomas D, Lipp P, Tovey SC, Berridge MJ, Li W, Tsien RY, Bootman MD (2000) Microscopic properties of elementary Ca<sup>2+</sup> release sites in non-excitable cells. *Curr Biol* 10(1):8–15
- [136] Thul R, Bellamy TC, Roderick HL, Bootman MD, Coombes S (2008) Calcium oscillations. *Adv Exp Med Biol* 641:1–27
- [137] Thurley K, Skupin A, Thul R, Falcke M (2012) Fundamental properties of Ca<sup>2+</sup> signals. *Biochim Biophys Acta* 1820(8):1185–94
- [138] Toyoshima C (2008) Structural aspects of ion pumping by Ca<sup>2+</sup>-ATPase of sarcoplasmic reticulum. *Arch biochem biophys* 476(1):3–11
- [139] Tsai J, Sneyd J (2005) Existence and stability of traveling waves in buffered systems. *SIAM J Appl Math* 66(1):237–265
- [140] Tsai JC, Sneyd J (2007) Are buffers boring? Uniqueness and asymptotical stability of traveling wave fronts in the buffered bistable system. *J Math Biol* 54(4):513–53, DOI [10.1007/s00285-006-0057-3](https://doi.org/10.1007/s00285-006-0057-3)
- [141] Tsai JC, Sneyd J (2011) Traveling waves in the buffered FitzHugh-Nagumo model. *SIAM J Appl Math* 71(5):1606–1636
- [142] Tsai JC, Zhang W, Kirk V, Sneyd J (2012) Traveling waves in a simplified model of calcium dynamics. *SIAM J Appl Dyn Syst* 11(4):1149–1199, DOI [10.1137/120867949](https://doi.org/10.1137/120867949)
- [143] Tsaneva-Atanasova K, Osinga HM, Riess T, Sherman A (2010a) Full system bifurcation analysis of endocrine bursting models. *J Theor Biol* 264(4):1133–46
- [144] Tsaneva-Atanasova K, Osinga HM, Tabak J, Pedersen MG (2010b) Modeling mechanisms of cell secretion. *Acta Biotheoretica* 58(4):315–327
- [145] Tuan HT, Williams GS, Chikando AC, Sobie EA, Lederer WJ, Jafri MS (2011) Stochastic simulation of cardiac ventricular myocyte calcium dynamics and waves. *Conf Proc IEEE Eng Med Biol Soc* 2011:4677–80
- [146] Ventura AC, Sneyd J (2006) Calcium oscillations and waves generated by multiple release mechanisms in pancreatic acinar cells. *Bull Math Biol* 68(8):2205–31, DOI [10.1007/s11538-006-9101-0](https://doi.org/10.1007/s11538-006-9101-0)
- [147] Wagner J, Keizer J (1994) Effects of rapid buffers on Ca<sup>2+</sup> diffusion and Ca<sup>2+</sup> oscillations. *Biophys J* 67:447–456
- [148] Wagner LE, Yule DI (2012) Differential regulation of the InsP<sub>3</sub> receptor type-1 and -2 single channel properties by InsP<sub>3</sub>, Ca<sup>2+</sup> and ATP. *J Physiol* 590(14):3245–3259
- [149] Wang IY, Bai Y, Sanderson MJ, Sneyd J (2010) A mathematical analysis of agonist- and KCl-induced Ca<sup>2+</sup> oscillations in mouse airway smooth muscle cells. *Biophys J* 98(7):1170–1181
- [150] Wechselberger M (2012) A propos de canards (apropos canards). *Trans Amer Math Soc* 364:3289–3309
- [151] Williams GS, Chikando AC, Tuan HT, Sobie EA, Lederer WJ, Jafri MS (2011) Dynamics of calcium sparks and calcium leak in the heart. *Biophys J* 101(6):1287–96

- [152] Williams GSB, Molinelli EJ, Smith GD (2008) Modeling local and global intracellular calcium responses mediated by diffusely distributed inositol 1,4,5-trisphosphate receptors. *J Theor Biol* 253(1):170–88
- [153] Winslow RL, Greenstein JL (2013) Extinguishing the sparks. *Biophys J* 104(10):2115–7
- [154] Yao Y, Choi J, Parker I (1995) Quantal puffs of intracellular  $\text{Ca}^{2+}$  evoked by inositol trisphosphate in *Xenopus* oocytes. *J Physiol* 482 ( Pt 3):533–53
- [155] Yule DI (2010) Pancreatic acinar cells: molecular insight from studies of signal-transduction using transgenic animals. *Int J Biochem Cell Biol* 42(11):1757–61
- [156] Zhang M, Goforth P, Bertram R, Sherman A, Satin L (2003) The  $\text{Ca}^{2+}$  dynamics of isolated mouse beta-cells and islets: implications for mathematical models. *Biophys J* 84(5): 2852–2870
- [157] Zhang W, Kirk V, Sneyd J, Wechselberger M (2011) Changes in the criticality of Hopf bifurcations due to certain model reduction techniques in systems with multiple timescales. *J Math Neurosci* 1(1):9
- [158] Zhang W, Krauskopf B, Kirk V (2012) How to find a codimension-one heteroclinic cycle between two periodic orbits. *Discrete Cont Dyn S* 32(8):2825–2851

Mathematical Analysis of Complex Cellular Activity

Bertram, R.; Tabak, J.; Teka, W.; Vo, T.; Wechselberger, M.; Kirk, V.; Sneyd, J.

2015, XII, 107 p. 37 illus., 25 illus. in color., Softcover

ISBN: 978-3-319-18113-4